

On the Molecular Basis of Ion Permeation in the Epithelial Na⁺ Channel

Stephan Kellenberger, Nicole Hoffmann-Pochon, Ivan Gautschi, Estelle Schneeberger, and Laurent Schild

From the Institut de Pharmacologie et de Toxicologie, Université de Lausanne, CH-1005 Lausanne, Switzerland

abstract The epithelial Na⁺ channel (ENaC) is highly selective for Na⁺ and Li⁺ over K⁺ and is blocked by the diuretic amiloride. ENaC is a heterotetramer made of two α , one β , and one γ homologous subunits, each subunit comprising two transmembrane segments. Amino acid residues involved in binding of the pore blocker amiloride are located in the pre-M2 segment of β and γ subunits, which precedes the second putative transmembrane α helix (M2). A residue in the α subunit (α S589) at the NH₂ terminus of M2 is critical for the molecular sieving properties of ENaC. ENaC is more permeable to Li⁺ than Na⁺ ions. The concentration of half-maximal unitary conductance is 38 mM for Na⁺ and 118 mM for Li⁺, a kinetic property that can account for the differences in Li⁺ and Na⁺ permeability. We show here that mutation of amino acid residues at homologous positions in the pre-M2 segment of α , β , and γ subunits (α G587, β G529, γ S541) decreases the Li⁺/Na⁺ selectivity by changing the apparent channel affinity for Li⁺ and Na⁺. Fitting single-channel data of the Li⁺ permeation to a discrete-state model including three barriers and two binding sites revealed that these mutations increased the energy needed for the translocation of Li⁺ from an outer ion binding site through the selectivity filter. Mutation of β G529 to Ser, Cys, or Asp made ENaC partially permeable to K⁺ and larger ions, similar to the previously reported α S589 mutations. We conclude that the residues α G587 to α S589 and homologous residues in the β and γ subunits form the selectivity filter, which tightly accommodates Na⁺ and Li⁺ ions and excludes larger ions like K⁺.

key words: epithelial Na⁺ channel • *Xenopus* oocyte • pore • selectivity • ion channel

introduction

The highly selective epithelial sodium channel (ENaC)¹ in the apical membrane of epithelial cells represents the predominant pathway in mediating sodium reabsorption in the distal nephron, the colon, and the lung (Garty and Palmer, 1997). This electrogenic vectorial transport of Na⁺ is accomplished by a two-step transport system involving the apical ENaC and the basolateral Na⁺-K⁺ pump. In the distal nephron, ENaC activity is regulated by aldosterone and vasopressin, serving to maintain Na⁺ balance, extracellular volume, and blood pressure. The functional characteristics of ENaC have been studied in isolated renal tubular segments and in recombinant expression systems using patch-clamp techniques. ENaC is a small 4–6-pS conductance channel in isotonic NaCl with high selectivity for Na⁺ and Li⁺ over K⁺ (permeability ratios $P_{\text{Li}}/P_{\text{Na}} > 1$ and $P_{\text{Na}}/P_{\text{K}} > 100$) and slow gating kinetics. ENaC currents are blocked by submicromolar concentrations of amiloride.

Portions of this work were previously published in abstract form (Kellenberger, S., N. Hoffmann-Pochon, E. Schneeberger, I. Gautschi, and L. Schild. 1998. *J. Am. Soc. Nephrol.* 9: A0193).

Address correspondence to Laurent Schild, Institut de Pharmacologie et de Toxicologie, Bugnon 27, CH-1005 Lausanne, Switzerland. Fax: 4121 692 5355; E-mail: laurent.schild@ipharm.unil.ch

¹Abbreviations used in this paper: 3B2S, three-barrier-two-site; ENaC, epithelial Na⁺ channel; I/V, current-voltage; K_M , ion concentration for half-maximal unitary conductance; wt, wild type.

ENaC belongs to a new class of channel proteins called the ENaC/DEG superfamily, which includes a variety of proteins involved in mechanotransduction and neurotransmission, and is found in nematodes, flies, snails, and mammals (for review see Tavernarakis and Driscoll, 1997; Waldmann and Lazdunski, 1998). Subunits of this superfamily coassemble usually within subfamilies into Na⁺-preferring or -selective multimeric channels that are either constitutively active (e.g., ENaC), activated by mechanical stimuli (as postulated for *Caenorhabditis elegans* degenerins), activated by a peptide (FMRFamide peptide-gated Na⁺ channel, FANaC; Lingueglia et al., 1995), or activated by protons (ASIC).

ENaC is a heterotetramer, and made of two α , one β , and one γ homologous subunits arranged around the channel pore in an $\alpha\beta\alpha\gamma$ configuration (Canessa et al., 1994b; Firsov et al., 1998). Each homologous subunit has two transmembrane spanning segments (M1 and M2) with intracellular NH₂ and COOH termini leaving a large extracellular hydrophilic loop, as illustrated in Fig. 1 A (Canessa et al., 1994a; Renard et al., 1994). Based on sequence comparisons, current models predict that the second transmembrane spanning segment of ENaC forms an α helix starting with a conserved Ser residue (α S589) and extending 22 residues further downstream in the defined ENaC sequence (see Fig. 1 B). A pre-M2 segment can arbitrarily be defined as a sequence delineated by a conserved Gly (α G579) residue

at the 5' end and α S589 at the 3' end that initiates the M2 segment. Fig. 1 C shows a model of the narrow pore region of ENaC, based on this and previous work. Previous mutagenesis experiments provided evidence that the pre-M2 forms the outer pore of ENaC (Schild et al., 1997). Amino acid residues mutated in those experiments are presented in bold on a gray background in Fig. 1 B. These experiments showed that mutations of Gly residues in β (G525) and γ (G537) subunits decrease the affinity for the pore blocker amiloride and change single-channel conductance. In addition, a Cys substitution at the homologous position of α ENaC (α S583C) generated a high affinity Zn^{2+} binding site that leads to channel block by Zn^{2+} . Recently, we have shown that mutations of the conserved Ser residue α S589 allow larger ions such as K^+ , Rb^+ , and Cs^+ as well as divalent cations to pass through the channel (Kellenberger et al., 1999). Ion substitution experiments indicate that α S589 determines the molecular cutoff of the channel pore at its narrowest point, the selectivity filter. Thus, in the pre-M2 segment that lines the outer channel pore, the amiloride binding site precedes the selectivity filter in the sequence.

In this study, we have analyzed the role of conserved amino acid residues located between the amiloride binding site (corresponding to α S583) and the selectivity filter (α S589) in channel permeation properties and blocking by amiloride. We have focused our interest on the conserved aromatic residues at the position corresponding to W585 in the α ENaC sequence, and on a cluster of Ser and Gly residues (α G587, α S588, and analogous amino acids in β and γ subunits; see Fig. 1 B).

methods

Site-directed Mutagenesis

Mutations were introduced in rat ENaC cDNA as described previously (Schild et al., 1997). Complementary RNAs of each α , β , γ subunit were synthesized *in vitro*. For binding experiments, α , β , and γ subunits that had been tagged as described by Firsov et al. (1996) were used with the FLAG reporter octapeptide in the extracellular loop, directly COOH terminal of the first transmembrane segment of each subunit. Healthy stage V and VI *Xenopus* oocytes were pressure injected with 100 nl of a solution containing equal amounts of $\alpha\beta\gamma$ ENaC subunits at a total concentration of 100 ng/ μ l. For simplicity, ENaC mutants are named by the mutated subunit only, although always all three subunits (α , β , and γ) were coexpressed.

Binding Experiments

The FLAG reporter octapeptide, which had been introduced in α , β , and γ subunits, is recognized by the anti-FLAG M_2 mouse monoclonal antibody (M_2 Ab) (Eastman Kodak Co.). M_2 Ab was iodinated as described by Firsov et al. (1996). Iodinated M_2 Ab had a specific activity of $5\text{--}20 \cdot 10^{17}$ cpm/mol and were used up to 2 mo after synthesis. On the day after mRNA injection, oocytes were transferred to a 2-ml Eppendorf tube containing modified Barth's saline (mM: 10 NaCl, 90 *N*-methyl-d-glutamine HCl, 0.8

MgSO₄, 0.4 CaCl₂, 5 HEPES, pH 7.2) supplemented with 10% heat-inactivated calf serum, and incubated for 30 min on ice. The binding was started upon addition of 12 nM ¹²⁵I- M_2 Ab (final concentration) in a volume of 5–6 μ l/oocyte. After 1 h of incubation on ice, the oocytes were washed eight times with 1 ml modified Barth's saline supplemented with 5% heat-inactivated calf serum, and then transferred individually into tubes for γ counting containing 250 μ l of the same solution. The samples were counted and the same oocytes were kept for subsequent measurement of the whole-cell current. Nonspecific binding was determined from parallel assays of noninjected oocytes. Theoretically, it might be possible that our mutations affect the accessibility of the FLAG epitope for the M_2 antibody by changing the conformation of the extracellular loop. However, this possibility seems rather unlikely since most of the mutations did not affect ¹²⁵I- M_2 Ab binding.

Electrophysiological Recording

Electrophysiological measurements were taken at 16–20 h after injection. Two-electrode voltage-clamp recordings were obtained using a TEV-200 amplifier (Dagan Corp.). The standard bath solution contained 110 mM NaCl, 1.8 mM CaCl₂, 10 mM HEPES-NaOH, pH 7.35. For selectivity measurements, Na⁺ was replaced by Li⁺, K⁺, Rb⁺, or Cs⁺ at the same concentration. Macroscopic amiloride-sensitive currents (I) are defined as the difference between ionic currents obtained in the presence and absence of 5 μ M (or higher concentrations for some mutants, as indicated) of amiloride (Sigma Chemical Co.) in the bath. All macroscopic currents shown are amiloride-sensitive currents as defined above. Pulses for current–voltage curves were applied, and data were acquired using a PC-based data acquisition system (Pulse; HEKA Elektronik).

The cell-attached or outside-out configuration of the patch-clamp technique was used to obtain macropatch and single-channel data. Before recording, the vitelline layer of the oocyte was removed. For cell-attached patches, the oocytes were kept in a standard bath K⁺ solution to depolarize the membrane potential, and pipette solutions were Na⁺ or Li⁺, as described above. For outside-out patches, extracellular solutions were as described above. Changes of external solutions of outside-out patches were made using the Rapid Solution Changer RSC-200 (BioLogic International Ltd.). In this system, the perfusion solutions are driven by gravity to the rotating head containing in these experiments up to 11 glass tubes. The solution exchange is performed by a highly precise and fast rotation of the RSC head, which exposes the patch pipette to the flow of one of the tubes. Times of rotation from one tube to the adjacent one were a few milliseconds. The pipet solution contained 75 mM CsF, 17 mM *N*-methyl-d-glucamine, 10 mM EGTA, and 10 mM HEPES, pH 7.35. Pipettes were pulled from Borosilicate glass (World Precision Instruments, Inc.). In patch-clamp experiments, currents were recorded with a List EPC-9 patch clamp amplifier (HEKA Elektronik) and filtered at 100 Hz for analysis. Data are shown as mean \pm SEM, or as indicated.

Data Analysis

To analyze titration curves for inhibition of macroscopic Li⁺ or Na⁺ currents (I), the ratio I/I₀ measured in the presence (I) of a particular blocker B to that in the absence of the blocker (I₀) is described by the inhibition equation: $I/I_0 = K_i^{n'} / (K_i^{n'} + [B]^{n'})$, where K_i is the inhibitory constant of the blocker, [B] is the concentration of the blocker, and n' is a pseudo-Hill coefficient. For the fit of Li⁺ block of Na⁺ current through γ S541A ENaC (see Fig. 8), n' was set equal to 1, and a nonblockable fraction of the amiloride-sensitive current (I) was introduced. This nonblock-

able fraction of I was set equal to the amiloride-sensitive current carried by 140 mM Li^+ alone, normalized to the amiloride-sensitive current carried by 20 mM Na^+ (e.g., 0.21 ± 0.01 at -150 mV, $n = 6$).

Modeling of Energy Barrier Profiles

A reaction rate theory treatment of transmembrane ionic diffusion considers ion movement as a series of discrete steps between energy minima (wells) separated by energy maxima (barriers). One may simply account for saturation or ionic block by assuming that only one ion at a time may reside in a particular energy well, which corresponds to a discrete ion-binding site in the channel, and that individual ions cannot pass each other in the channel. To fit our current-voltage (I/V) data collected at various Na^+ or Li^+ concentrations to discrete-state barrier models, we have used a version of the AJUSTE program, originally developed by Alvarez et al. (1992) and modified by French et al. (1994). The theoretical basis of barrier models is described extensively in Alvarez et al. (1992), French et al. (1994), and Hille (1992). We used a discrete-state permeation model based on a kinetic scheme for a three-barrier-two-site (3B2S) channel that includes double-ion occupancy and ion-ion repulsion.

The energy diagram in Fig. 9 A (below) summarizes the adjustable parameters of the model. The energies of the unoccupied channel at zero voltage are defined by three peak energies (G_1 , G_2 , and G_3) and two wells or site energies (U_1 and U_2) for Na^+ and Li^+ . The subscripts of the parameters refer to the position with respect to the inside solution as shown in Fig. 9 A. The program can deal with the simultaneous presence of three types of ions. The distances D_1 – D_6 refer to the fraction of the electric field that separates peak and well positions with the requirement that $D_1 + D_2 + D_3 + D_4 + D_5 + D_6 = 1$. In addition to the above energy and distance parameters, there is an interaction energy A (ion x , ion y), which models the effects of ion-ion interactions between the same or different types of ions. The reference energy state used in the model is 1 mol fraction, which corresponds to 55.5 M. Conversion to a 1-M reference state is readily accomplished by addition of 4.0 RT units to the reported peak and well energies. The translocation rate constant K for translocation from well U over peak G is related to the translocation barrier height ($\Delta G = G_G - G_U$) according to $K = (kT/h) \exp(-\Delta G/RT)$, where k is Boltzmann's constant, T is the temperature in $^\circ\text{K}$, and h is Planck's constant ($kT/h = 6.2 \times 10^{12} \text{ s}^{-1}$ at 25°C).

For the modeling of energy barrier profiles, we used single-channel data from outside-out patches of *Xenopus* oocytes expressing wild-type (wt) or mutant ENaC. Data sets had been obtained at three to five different negative membrane potentials (less than -50 and more than -180 mV) and four to six different external concentrations of the permeant ion (either Na^+ or Li^+ at 15–200 mM) per channel type, and in the absence of any permeant ions in the internal solution. As we have analyzed inward, but not outward, currents for the modeling, the part of the energy barrier profiles on the extracellular side (G_2 , G_3 , U_2) are well defined, whereas the quality of the fit was relatively insensitive to changes of the energy parameters U_1 and G_1 . The procedure for fitting single channel data consisted first in setting barrier profiles for ENaC wt with either Na^+ or Li^+ as the single permeant ion. The quality of fits was evaluated both visually and by SUMSQ, which is the weighted sum of squared differences between experimental and theoretical data minimized by the fitting routine. The parameter values for the electrical distance D were arbitrarily constrained by a requirement of symmetry about the central barrier located at an electrical distance of 0.5. The optimal arrangement found for wt ENaC was $D_1 = D_6 = 0.1$, $D_2 =$

$D_5 = 0.15$, and $D_3 = D_4 = 0.25$, and this arrangement was used for fitting of all mutants. The quality of the fit was relatively insensitive to the ion-ion interaction parameter A . This can be readily explained by the fact that the data used for constructing the model was obtained at relatively low ion concentrations (typically <160 mM). In this concentration range, the probability of double occupancy of the channel was <0.01 , even with A set to a low value (2.6). This is consistent with flux-ratio experiments indicating that ENaC forms a one-ion pore (Palmer, 1982).

The model obtained for Na^+ permeation of wt channels is shown in Fig. 9 B (below). The model fits the conductance/ion concentration relationship well, as shown by the comparison of model prediction (solid line) and data points (symbols) in Fig. 7 (below). The outer well (U_2) is deeper than the inner well (U_1). This difference allowed fitting of mutant data, in which the apparent channel affinity for Na^+ decreased (γS541A , αG587A) by just changing one well energy (one binding site) with regard to wt. This energy profile predicts an almost ohmic behavior of the channel, with outward currents $<111\%$ and $>90\%$ of inward currents over a voltage range of ± 150 mV. Based on the energy profile obtained for the wt Na^+ permeation, the profile best suited for Li^+ permeation of wt ENaC was obtained by increasing U_2 and G_3 (see Figs. 7 and 9 A). Starting from these two models for Li^+ and Na^+ permeation, we attempted to fit the mutant data by changing only energy values of one well and one barrier at the extracellular side of the permeation pathway, either U_2 and G_2 , or U_2 and G_3 , assuming that single point mutations in the external channel pore would not affect binding sites on both sides of the highest barrier of the selectivity filter. Adjustment of at least one barrier was necessary to adjust the model to the experimental conductance values. By changing U_2 and G_2 , we obtained better fits of our experimental data than by changing U_2 and G_3 . For this reason, we report here models obtained by only the first method.

Finally, we used the 3B2S model to fit the block of 20 mM Na^+ currents in the γS541A mutant by increasing Li^+ concentrations (see Fig. 8). In this case, the model takes into account the simultaneous presence of Na^+ and Li^+ in the external solution. The use of the 3B2S model requires that macroscopic currents are converted to unitary currents. The macroscopic current data of Li^+ block in macropatches were normalized at each voltage to the condition with 20 mM Na^+ alone and, for each voltage, these normalized currents were multiplied by the single-channel current for 20 mM Na^+ predicted by the $\gamma\text{S541A-Na}^+$ model. These modified data were then used to obtain a model for Li^+ permeation of the γS541A channel.

results

The sequence alignment of the pre-M2 segment and the NH_2 -terminal part of M2 of ENaC subunits and homologous proteins is illustrated in Fig. 1 B. Residues, which have previously been shown to be important for ion permeation and/or blocking of ENaC currents by amiloride are shown in bold on a gray background and amino acids that have been analyzed in the present study are shown in white on a dark background. αS583 and the corresponding residues βG525 and γG539 line the outer channel pore as shown in Fig. 1 C at a site where amiloride plugs the channel (Schild et al., 1997). αS589 at the NH_2 terminus of M2 is part of the narrowest region of the pore at the selectivity filter (Kellenberger et al., 1999). Other amino acid residues

T A B L E I
Cell Surface Expression and Apparent Affinities to Amiloride of Mutant and wt ENaC

| | K_i amiloride | I_{Na} | Binding ratio cpm total/ cpm nonspecific | | K_i amiloride | I_{Na} | Binding ratio cpm total/ cpm nonspecific |
|----------------|------------------|----------------|---|------------------|------------------|-----------------|---|
| | μM | μA | | | μM | μA | |
| α W585A | 0.17 ± 0.07 | 5.1 ± 1.1 | | γ S541A | 0.05 ± 0.01 | 6.1 ± 3.4 | 4.5 ± 2.5 |
| α W585C | 0.20 ± 0.06 | 10.8 ± 2.9 | | γ S541G | 0.14 ± 0.01 | 25.2 ± 3.4 | |
| α W585E | 0.13 ± 0.05 | 10.6 ± 1.6 | | γ S541N | ND | 0 | 4.0 ± 2.0 |
| α W585R | 0.22 ± 0.04 | 4.3 ± 2.0 | | γ S541F | ND | 0 | 4.6 ± 1.5 |
| β W527A | ND | 0 | 2.1 ± 0.8 | γ S541R | ND | <0.3 | 3.3 ± 1.1 |
| β W527C | 0.13 ± 0.02 | 5.2 ± 3.7 | | α S588A | 0.30 ± 0.06 | 14 ± 7.5 | |
| β W527E | 0.07 ± 0.05 | 4.6 ± 1.9 | | α S588I | 2.06 ± 0.17 | 9.2 ± 7.2 | |
| β W527R | 0.25 ± 0.02 | 0.4 ± 0.2 | 1.5 ± 0.5 | β G530A | 0.16 ± 0.05 | 4.0 ± 1.1 | |
| γ W539A | 0.14 ± 0.03 | 11.1 ± 9.2 | | γ C542A | 0.10 ± 0.04 | 6.7 ± 5.4 | |
| γ W539C | 0.14 ± 0.03 | 9.8 ± 4.7 | | | | | |
| γ W539E | 0.11 ± 0.02 | 4.3 ± 1.3 | | α V590A | 0.28 ± 0.08 | 15.5 ± 3.2 | |
| γ W539R | 0.54 ± 0.05 | 0.4 ± 0.0 | 1.2 ± 0.7 | β V532A | 0.12 ± 0.03 | 8.9 ± 1.7 | |
| α G587A | 0.03 ± 0.01 | 3.7 ± 2.7 | 8.2 ± 3.6 | γ V544A | 0.20 ± 0.04 | 11.2 ± 2.7 | |
| α G587D | ND | 0 | 5.5 ± 1.1 | | | | |
| α G587S | 0.75 ± 0.03 | 7.1 ± 1.2 | | α DEL * | ND | 0 | 0.9 ± 0.4 |
| β G529A | 4.26 ± 0.74 | 3.5 ± 2.7 | 9.6 ± 4.8 | α H282D * | 0.27 ± 0.024 | 17.0 ± 11.3 | |
| β G529C | 5.31 ± 1.92 | 2.5 ± 1.8 | | α K550E * | 0.15 ± 0.01 | 13.7 ± 8.5 | |
| β G529S | 13.82 ± 0.21 | 4.8 ± 0.7 | | α K561E * | 0.23 ± 0.03 | 38.0 ± 8.2 | |
| β G529D | 0.07 ± 0.01 | 0.6 ± 0.4 | | | | | |
| β G529R | 0.05 ± 0.01 | 2.6 ± 1.7 | 7.2 ± 4.8 | wt | 0.11 ± 0.02 | 2.9 ± 1.3 | 8.4 ± 3.9 |

K_i values were calculated from two-electrode voltage-clamp recordings in *Xenopus* oocytes, at -100 mV in extracellular solutions containing either 20 mM Na^+ or Li^+ (see methods) $n = 5-12$, errors are SEM returned from the fit routine. Cell surface expression was determined as binding of an iodinated antibody to intact oocytes, as described in methods. Errors for binding data are SD, $n = 15-30$.

in this region, α W585 and α V590 and their analogues in β and γ subunits, are conserved and might be important for the ion permeation properties. We have mutated the α W585, β W527, and γ W539 residues to various amino acids and did not observe any significant changes in ion selectivity, unitary conductance, or block by amiloride (Tables I-III). The level of cell surface expression of wt and mutant ENaC was determined on intact oocytes by specific binding of an iodinated monoclonal antibody to a FLAG epitope inserted in the extracellular domain of ENaC subunits (see methods). Some mutations resulted in a low expression of the channel at the cell surface (Table I). Similar to Trp mutations, Ala substitutions of the conserved α V590, β V532, and γ V544 residues were without effects on the biophysical and pharmacological properties of the channel (Tables I-III). This lack of effects of mutations of the conserved Trp and Val residues suggests that these amino acids may not line the channel pore.

Next, we looked at the cluster of Ser and Gly residues, α G587 and α S588 and the analogous amino acid residues in β and γ subunits (Fig. 1 B). The α S588I mutation is known to increase single channel conductance for Na^+ ions and to decrease channel affinity for blocking by amiloride (Waldmann et al., 1995b; Tables I-III).

More conserved mutations, however, such as Ala substitutions of α S588 and the homologous residues β G530 and γ C542 did not change ion conductance properties or channel affinity for amiloride (Tables I-III). The effect of α S588I on channel conductance corroborates the previous observation that α S588 is close to the selectivity filter (Kellenberger et al., 1999).

Mutations of α G587, β G529, and γ S541 Change Ion-permeation Properties and Channel Block by Amiloride

Conserved Gly residues in the α and β subunits at positions α 587 and β 529, and the unique Ser residue in the γ subunit (γ S541) were substituted with the polar Ser, the nonpolar residues Cys, Gly, or Ala or the negatively charged Asp. Analysis of the concentration-dependent block of macroscopic Na^+ currents by amiloride (Table I) showed that specific mutations in α and β subunits decreased channel affinity for amiloride. The β G529A, β G529S, and β G529C mutations resulted in a 40- to 130-fold increase in K_i for amiloride, and a significant sevenfold increase in amiloride K_i was measured for α G587S. Some substitutions of these residues had no effect on block by amiloride (α G587A, β G529D, β G529R; Table I), suggesting that these amino acids

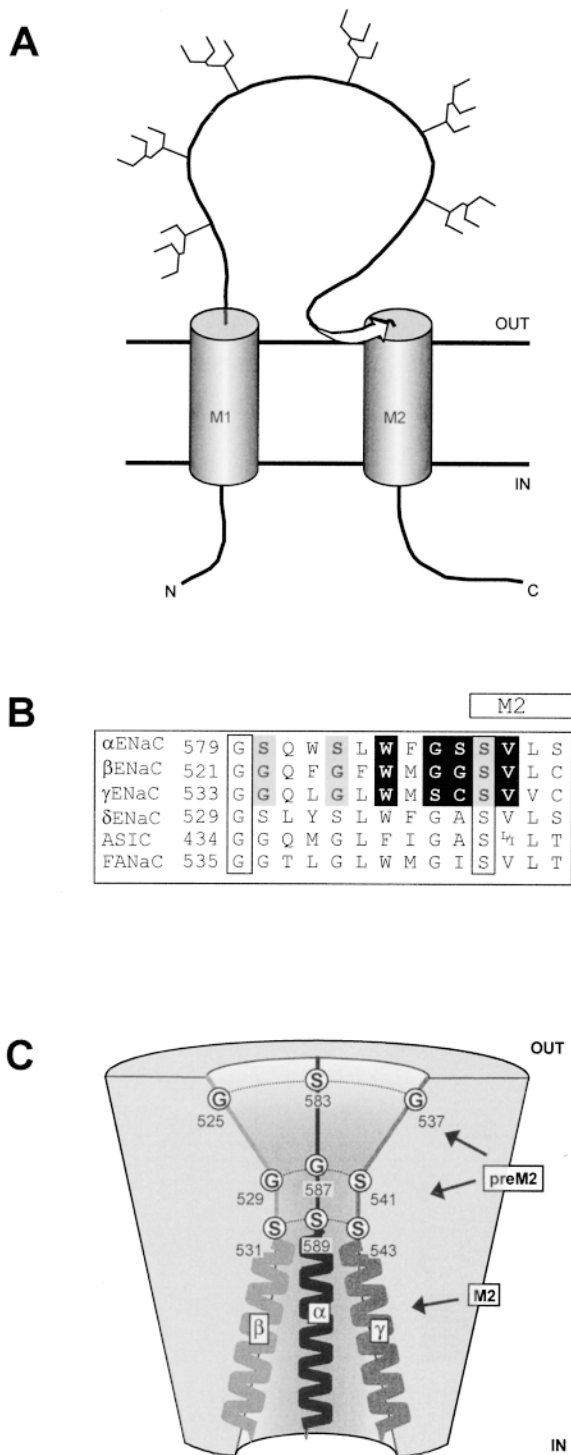


Figure 1. Sequence alignment and structural model of the pore region of ENaC. (A) Linear model of an ENaC subunit showing two transmembrane domains, M1 and M2, with a pre-M2 segment. (B) Sequence alignment of the pre-M2 segments of α , β , γ , δ ENaC, the ASIC family, and FANaC (FMRFamide peptide-gated Na^+ channel; Waldmann et al., 1995a) (Waldmann and Lazdunski, 1998; Tavernarakis and Driscoll, 1997). The number of the first residue shown of rat α , β , γ ENaC, human δ ENaC, rat ASIC1, and FANaC is indicated. The putative start of M2, as predicted by the PHDhtm (transmembrane helix location) program at EMBL-

are not part of the amiloride binding site, but rather are indirectly involved in channel block.

No I_{Na} was detected for α G587D and γ S541N or γ S541F mutants, and only a small I_{Na} ($<0.3 \mu\text{A}$) was detected for γ S541R even using high (1 mM) amiloride or benzamil concentrations. In the case of the α G587D mutant, I_{Na} was not detected despite a 5.5-fold higher anti-FLAG binding signal compared with the background signal. The specific anti-FLAG binding to oocytes expressing the α G587D mutant was only slightly lower than binding to oocytes expressing the functional α G587A mutant (Table I). Similarly, specific anti-FLAG antibody binding was about the same for the nonconducting γ S541N and γ S541F mutants and for γ S541R compared with the functional γ S541A mutant (Table I). These observations indicate that α G587D, γ S541N, γ S541F, and γ S541R mutants are expressed at the cell surface, but are nonconducting channels or channels with minuscule conductance (γ S541R), consistent with the notion that mutations of α G587 and γ S541 residues affect ion permeation through the channel. Thus it appears that ENaC can tolerate relatively conservative substitutions at these positions and that less conservative replacements can make the channel nonfunctional.

We tested whether α G587A, β G529A, or γ S541A mutations affect channel selectivity for Li^+ over Na^+ ions. Representative current traces in the presence of extracellular Na^+ solution at different voltages are shown in Fig. 2, A and B, for wt and the γ S541A mutant. When Li^+ replaced Na^+ in the external medium, the amiloride-sensitive inward current increased in oocytes expressing ENaC wt (Fig. 2 A), but clearly decreased in oocytes expressing γ S541A (Fig. 2 B). The macroscopic current-voltage relationships of ENaC wt and the α G587A,

Heidelberg, is indicated. The amino acid residues shown are identical within subunits across the species. Amino acid residues shown in open boxes are conserved across all known genes of the ENaC family. Amino acids analyzed in this study are shown in white on a dark background. Amino acids whose function has been analyzed in previous studies are shown in bold on gray background. α S583 and the homologous amino acid residues β G525 and γ G537 change channel affinity for amiloride block (Schild et al., 1997). α S589 is a determinant of the geometry of the narrowest part of the pore (Kellenberger et al., 1999). (C) The cross-section shows the pre-M2 segments and the second putative transmembrane α -helices (M2) of an α subunit (black, center), a β subunit (gray, on the left) and a γ subunit (dark gray, on the right). The second α subunit located on the side of the viewer (Firsov et al., 1998) is not shown. The outer vestibule is lined by the pre-M2 segment where amiloride binds to α S583 and the corresponding Gly residues in the β and γ subunit (Schild et al., 1997). The vestibule narrows down to the selectivity filter formed by α G587, β G529, and γ S541 residues and the ring of Ser residues (α S589 and analogues; Kellenberger et al., 1999).

TABLE II

Macroscopic Amiloride-sensitive Currents and Current Ratios at -100 mV

| | I_{Na} | n | I_{Li}/I_{Na} | n | I_K/I_{Na} | n |
|----------------|-----------------|-----|-----------------|-----|-------------------|-----|
| α W585A | 15.6 ± 4.1 | 5 | 1.3 ± 0.2 | 5 | $-0.03 \pm 0.0^*$ | 5 |
| α W585C | 44.1 ± 13.7 | 7 | $1.0 \pm 0.1^*$ | 7 | 0.00 ± 0.0 | 4 |
| α W585E | 20.1 ± 13.5 | 7 | 1.2 ± 0.2 | 7 | 0.00 ± 0.0 | 4 |
| α W585R | 10.6 ± 6.1 | 7 | $1.1 \pm 0.1^*$ | 7 | 0.00 ± 0.0 | 4 |
| β W527C | 33.4 ± 11.7 | 7 | $1.1 \pm 0.1^*$ | 7 | 0.00 ± 0.0 | 4 |
| β W527E | 1.3 ± 1.9 | 12 | 1.5 ± 0.4 | 12 | 0.00 ± 0.0 | 3 |
| β W527R | <0.3 | 3 | ND | | ND | |
| γ W539A | 5.8 ± 8.9 | 12 | $1.1 \pm 0.1^*$ | 12 | -0.01 ± 0.0 | 7 |
| γ W539C | 26.2 ± 12.0 | 3 | 1.1 ± 0.1 | 3 | ND | |
| γ W539E | 11.2 ± 3.9 | 7 | 1.3 ± 0.1 | 7 | 0.00 ± 0.0 | 3 |
| γ W539R | <0.3 | 3 | ND | | ND | |
| α G587A | 6.6 ± 4.0 | 11 | $1.0 \pm 0.1^*$ | 3 | 0.01 ± 0.0 | 7 |
| α G587S | 2.0 ± 1.4 | 8 | 1.6 ± 0.2 | 8 | 0.01 ± 0.0 | 7 |
| β G529A | 10.9 ± 4.4 | 9 | $0.3 \pm 0.2^*$ | 9 | 0.00 ± 0.0 | 6 |
| β G529S | 3.0 ± 1.7 | 20 | $2.2 \pm 0.2^*$ | 8 | $0.22 \pm 0.2^*$ | 20 |
| β G529C | 1.4 ± 1.1 | 20 | $0.7 \pm 0.1^*$ | 8 | $0.06 \pm 0.0^*$ | 20 |
| β G529D | 0.3 ± 0.1 | 4 | 2.16 ± 0.2 | 4 | 0.19 ± 0.0 | 4 |
| β G529R | 1.3 ± 1.1 | 8 | $2.4 \pm 1.0^*$ | 8 | 0.02 ± 0.0 | 5 |
| γ S541A | 13.0 ± 6.1 | 5 | $0.2 \pm 0.0^*$ | 5 | 0.00 ± 0.0 | 4 |
| γ S541G | 5.5 ± 2.8 | 3 | $3.1 \pm 0.1^*$ | 3 | 0.00 ± 0.0 | 3 |
| α S588A | 42.8 ± 17.4 | 5 | 1.4 ± 0.1 | 5 | 0.01 ± 0.0 | 5 |
| α S588I | 7.9 ± 4.9 | 10 | $0.7 \pm 0.0^*$ | 3 | 0.00 ± 0.0 | 7 |
| β G530A | 38.6 ± 12.3 | 5 | 1.2 ± 0.1 | 5 | 0.01 ± 0.0 | 5 |
| γ C542A | 12.5 ± 12.9 | 7 | $1.9 \pm 0.5^*$ | 7 | 0.02 ± 0.0 | 1 |
| α V590A | 16.1 ± 8.0 | 5 | 1.7 ± 0.2 | 5 | 0.01 ± 0.0 | 3 |
| β V532A | 14.4 ± 15.5 | 6 | 1.3 ± 0.2 | 6 | 0.00 ± 0.0 | 4 |
| γ V544A | 6.0 ± 2.6 | 5 | 2.1 ± 0.4 | 5 | 0.00 ± 0.0 | 5 |
| α K550E | 38.3 ± 20.2 | 3 | 1.6 ± 0.2 | 3 | 0.00 ± 0.0 | 3 |
| α K561E | 50.7 ± 10.1 | 3 | 1.4 ± 0.2 | 3 | 0.00 ± 0.0 | 3 |
| α H282D | 17.0 ± 6.7 | 4 | 1.3 ± 0.1 | 4 | 0.00 ± 0.0 | 4 |
| wt | 27.5 ± 14.4 | 51 | 1.4 ± 0.3 | 39 | 0.00 ± 0.0 | 35 |

Amiloride-sensitive currents were measured in solutions containing 120 mM Na⁺, Li⁺, or K⁺. The amiloride concentration was 5 μ M, except for the mutants with low affinity to amiloride (see Table I), for which concentrations of 250 μ M were used. Errors are indicated as SD. *Ratio different from wt.

β G529A, or γ S541A mutants in the presence of external Na⁺, Li⁺, or K⁺ ions are plotted in Fig. 2 C. The currents of the I/V curves are normalized to I_{Na} of each channel type measured at -100 mV. In external Na⁺ solution, the I/V behavior of wt and mutant channels was identical. The I_{Li}/I_{Na} ratio was lower for the three mutants compared with wt, and followed the sequence wt > α G587A > β G529A > γ S541A. The current ratio I_{Li}/I_{Na} at -100 mV of all the α G587, β G529, and γ S541 mutants is shown in Table II. In addition to mutants shown in Fig. 2, β G529C also exhibited a decreased I_{Li}/I_{Na} ratio, whereas other mutants such as β G529D, β G529R, or γ S541G maintained I_{Li}/I_{Na} ratios > 1, similar to ENaC wt. Thus, the different effects by different β G529 substitutions cannot be correlated with properties of the amino acid side chain. The fact that substitu-

tion of β G529 by the much larger Arg did not change ion permeation indicates that the side chain may point away from the channel pore (see discussion).

The I/V relationship in external K⁺ did not provide evidence for a detectable K⁺ permeability for the α G587A, β G529A, and γ S541A mutants even at hyperpolarized membrane potentials (Fig. 2 C). However, β G529S generated a significant amiloride-sensitive inward K⁺ current as illustrated by the current-voltage behavior in Fig. 3. In the presence of external Na⁺ the I/V relationship of the β G529S mutant was identical to wt. When K⁺ replaced Na⁺ ions in the external medium, β G529S channels exhibited measurable inward currents at negative membrane potentials. At -100 mV, I_K represented 22% of I_{Na} ($I_K/I_{Na} = 0.22 \pm 0.2$, Table II). The β G529S mutant allows to a lesser extent Rb⁺ ions to pass through the channel ($I_{Rb}/I_{Na} = 0.04 \pm 0.01$, $n = 8$), but not larger ions like Cs⁺ ($I_{Cs}/I_{Na} < 0.01$, $n = 8$). The permeability of the β G529S mutant to K⁺ and Rb⁺ suggests that this mutation increased the molecular cutoff of the channel. Similarly, the β G529C mutant was also slightly permeant to larger ions with an I_K/I_{Na} ratio of 0.06 ± 0.0 (Table II) and an I_{Rb}/I_{Na} ratio of 0.03 ± 0.01 ($n = 8$). The β G529D mutant, which exhibited a I_K/I_{Na} ratio of 0.19 had a very low I_{Na} expression level and was not analyzed further. None of the α G587 or γ S541 mutants showed significant K⁺ permeability (Table II). We conclude from the analysis of these macroscopic current data that (a) the residues α G587 and β G529 in the pre-M2 segment play a role in channel block by amiloride, (b) α G587, β G529, and γ S541 are involved in defining channel Li⁺/Na⁺ permeability ratio, and (c) β G529 codetermines the molecular cutoff of the channel that normally prevents K⁺ ions from going through the channel.

Unitary Currents from α G587, β G529, and γ S541 Mutants

Measurements of channel unitary currents are necessary to ultimately demonstrate changes in ion permeation through the channel. Our single-channel analysis was focused mainly on channel mutants that exhibit important changes in macroscopic current properties. Many of the single-channel recordings were performed in the excised outside-out configuration to allow the determination of the channel sensitivity to amiloride to ascertain that unitary currents detected in the patch indeed represented the activity of ENaC mutants. Representative recordings are shown in Fig. 4. As anticipated from macroscopic currents, α G587A and β G529A showed reduced unitary currents with Li⁺ ions as charge carrier, and no obvious changes in unitary Na⁺ current (i_{Na}) or channel gating were observed. The corresponding γ S541A mutation decreased i_{Na} , and the unitary Li⁺ current (i_{Li}) was considerably reduced so that transitions between open and closed states could

TABLE III
Single-Channel Conductances and Conductance Ratios

| Mutant | Cell-attached patches | | | | Outside-out patches | | | |
|-----------------------------|-----------------------|---------------|-----------------|-----|---------------------|----------------|-----------------|-----|
| | g_{Na} | g_{Li} | g_{Li}/g_{Na} | n | g_{Na} | g_{Li} | g_{Li}/g_{Na} | n |
| | <i>pS</i> | <i>pS</i> | | | <i>pS</i> | <i>pS</i> | | |
| α W585E | 5.8 ± 0.6 | 8.4 ± 0.5 | 1.4 ± 0.2 | 5 | | | | |
| α W585R | 4.3 ± 0.2 | 7.4 ± 0.8 | 1.7 ± 0.3 | 4 | | | | |
| β W527E | | 6.4 ± 0.3 | | 3 | | | | |
| γ W539A | 5.6 ± 0.9 | 6.5 ± 0.7 | 1.2 ± 0.3 | 3 | | | | |
| γ W539C | | 7.9 ± 0.6 | | 5 | | | | |
| α G587A | | | | | 6.1 ± 0.5 | 6.9 ± 0.4 | 1.1 ± 0.2 | 3* |
| α G587S | | | | | 1.6 ± 0.1 | 3.2 ± 0.1 | 2.0 ± 0.2 | 4 |
| α G587D | | | | | | | | |
| β G529A | | | | | 6.1 ± 0.3 | 2.6 ± 0.2 | 0.4 ± 0.1 | 4* |
| β G529S | | | | | <1 pS | <1 pS | | 3 |
| β G529R | | | | | 6.0 ± 0.2 | 8.9 ± 0.2 | 1.5 ± 0.1 | 4 |
| γ S541A | | | | | 4.6 ± 0.2 | <1 pS | | 3* |
| γ S541G | | | | | 5.0 ± 0.6 | 8.8 ± 0.5 | 1.8 ± 0.3 | 4 |
| α S588A | | | | | 4.1 ± 0.3 | 7.8 ± 0.4 | 1.9 ± 0.2 | 3 |
| α S588I [†] | 10.0 ± 0.3 | 6.2 ± 0.2 | 0.6 ± 0.0 | 2 | | | | |
| | 11.9 ± 0.0 | 8.9 ± 0.7 | 0.7 ± 0.1 | 1 | | | | |
| β G530A | | | | | 3.4 ± 0.1 | 6.9 ± 0.4 | 2.0 ± 0.2 | 3 |
| γ C542A | | | | | 4.2 ± 0.2 | 10.2 ± 0.5 | 2.4 ± 0.2 | 3 |
| α V590A | | 7.6 ± 0.4 | | 3 | | | | |
| β V532A | 5.8 ± 0.7 | 8.4 ± 0.8 | 1.4 ± 0.3 | 2 | | | | |
| γ V544A | | | | | 4.7 ± 0.3 | 8.2 ± 0.9 | 1.7 ± 0.3 | 3 |
| α K550E | 5.5 ± 0.4 | 8.6 ± 0.3 | 1.5 ± 0.2 | 3 | | | | |
| α K561E | 4.0 ± 0.5 | 7.1 ± 0.5 | 1.8 ± 0.4 | 4 | | | | |
| wt | 5.2 ± 0.2 | 8.9 ± 0.7 | 1.7 ± 0.2 | 5 | 5.4 ± 0.2 | 9.1 ± 0.3 | 1.7 ± 0.1 | 4 |

g_{Na} , g_{Li} , single-channel conductance of Na^+ or Li^+ inward currents, respectively. *Conductance was measured at 100 mM extracellular Na^+ or 140 mM Li^+ , corresponding wt values are: 5.2 ± 0.2 pS (Na^+), 9.2 ± 0.3 (Li^+), and 1.8 ± 0.1 (g_{Li}/g_{Na} , $n = 4$). [†]Two different conductances were found for this mutant in one patch. The SEM of the g_{Li}/g_{Na} ratio was calculated as the sum of the fractional errors times the g_{Li}/g_{Na} ratio.

not be precisely determined under our recording conditions (Fig. 4). Single-channel conductance values, which are summarized in Table III, show that the unitary Li^+ conductance (g_{Li}) for the mutants follows the order $wt > \alpha$ G587A $>$ β G529A $>$ γ S541A. The g_{Li}/g_{Na} ratios agree with the Li^+/Na^+ permeability ratios measured for macroscopic amiloride-sensitive currents (Table II). The higher Li^+/Na^+ permeability of the β G529R and the γ S541G mutants compared with wt measured by the macroscopic I_{Li}/I_{Na} ratio ($I_{Li}/I_{Na} = 2.37$ and 3.11 , respectively, compared with 1.4 for wt), could not be confirmed by changes in either unitary currents for Na^+ or Li^+ ions, indicating that β G529R and γ S541G mutations do not increase channel permeability to Li^+ relative to Na^+ ions.

Comparison with other members of the ENaC gene family (Fig. 1 B) shows that at the position homologous to α G587 all known genes have a Gly residue, except for S541 in the ENaC γ subunit. Substitution of the γ S541 by Gly did not change the conductance or the ion selectivity of the channel. We also tested whether

Gly and Ser residues are interchangeable at the homologous positions in α and β subunits. The α G587S mutant showed a decreased unitary Na^+ and Li^+ conductance, but the g_{Li}/g_{Na} ratio remained unchanged (Table III). The most dramatic effect was observed with β G529S. As shown before (Fig. 3), this mutation makes the channel permeable to K^+ and preserves a macroscopic I_{Li}/I_{Na} ratio >1 . At the single-channel level, β G529S decreased unitary Na^+ and Li^+ current amplitudes to such an extent that transitions between open and closed states could not be detected. As shown in Fig. 5 in a representative experiment, channel openings or closures could not be detected under our conditions in excised outside-out patches containing channels with the β G529S mutation and exhibiting amiloride-sensitive Na^+ and Li^+ currents. This indicates that g_{Li} and g_{Na} of the β G529S mutant are more than likely <1 pS. Thus the analysis of the single-channel currents of the α G587, β G529, and γ S541 mutants indicate that substitution of these residues by Ala, Ser, or Cys change the ion permeation properties by decreasing channel

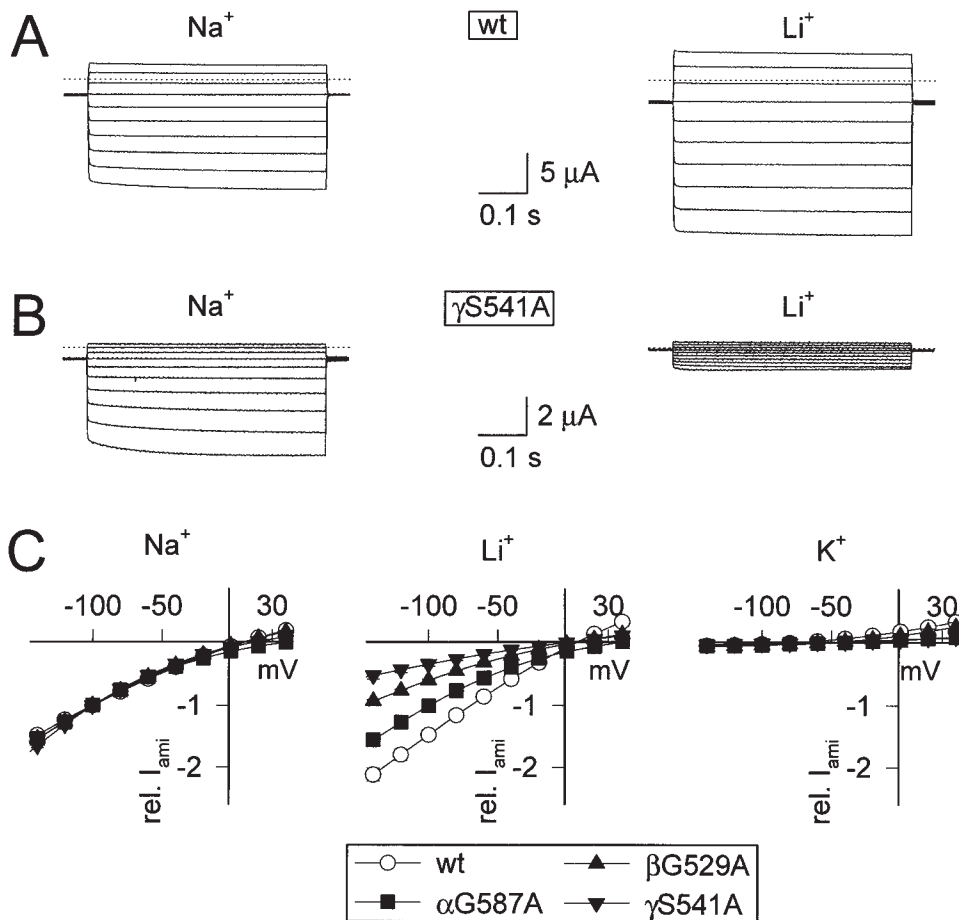


Figure 2. The macroscopic Li^+/Na^+ conductance ratio is decreased by mutations of homologous residues in α , β , and γ subunits. Current-voltage relationship of amiloride-sensitive currents in two-electrode voltage-clamp recordings from *Xenopus* oocytes. (A and B) Current traces of ENaC wt (A) and the γ S541A mutant (B) in 40 mM Na^+ or Li^+ solution. Currents were measured during 500-ms voltage steps from a holding potential of -20 mV to test potentials of -140 to $+40$ mV in 20-mV increments. Currents measured in the presence of amiloride were subtracted from currents measured in the absence of $5 \mu\text{M}$ amiloride, and these subtracted currents are shown. The dotted line indicates zero level of the amiloride-sensitive current. (C) Current-voltage relationship in 40 mM Li^+ , 40 mM Na^+ , or 120 mM K^+ bath solution from oocytes expressing wt, α G587A, β G529A, and γ S541A mutant ENaC are shown. Recordings were obtained as described in A and B, with the exception that $250 \mu\text{M}$ amiloride was used to block β G529A currents. For each oocyte, the

amiloride-sensitive current was normalized to the I_{Na} at -100 mV. I_{Na} at -100 mV was $13.9 \pm 2.3 \mu\text{A}$ for wt ($n = 17$), $3.3 \pm 0.7 \mu\text{A}$ for α G587A ($n = 9$), $11.1 \pm 1.0 \mu\text{A}$ for β G529A ($n = 12$), and $4.9 \pm 0.7 \mu\text{A}$ for the γ S541A mutant ($n = 10$).

conductances for either Li^+ ions alone or for both Li^+ and Na^+ .

Apparent Affinities for the Permeating Na^+ and Li^+ Ions of Mutants of the α G587, β G529, and γ S541 Residues

The decrease in unitary Li^+ current in the mutants reflects a slower movement of Li^+ ions along the pore of ENaC mutants. Strong binding interactions between the permeant ion and the residues lining the channel pore can account for a slow ion permeation through the pore. Alternatively, high energy barriers for ion translocation along the conduction pore are also expected to slow ion permeation. We addressed these possibilities by measuring the changes in unitary current i_{Na} and i_{Li} with increasing concentrations of the permeant ion, as illustrated in typical recordings in Fig. 6. From i_{Na} and i_{Li} measurements at different holding potentials, values for single-channel conductance (g_{Na} and g_{Li}) were obtained for ion concentrations ranging from 10 to 200 mM. Unitary conductances are plotted versus the concentration of the permeant ion (Na^+ or

Li^+) in Fig. 7. ENaC wt shows saturation of g_{Na} around 5 pS for Na^+ concentrations >100 mM, whereas g_{Li} does not saturate even at concentrations >100 mM. Values of ion concentration for half-maximal unitary conductance (K_{M}) were determined from fits of the conductance-ion concentration relationship to the Michaelis-Menten equation and are given in Table IV. In the case of ENaC wt, K_{M} values were 38 mM for Na^+ and 118 mM for Li^+ . The g_{Na} and g_{Li} saturation curves of wt ENaC suggest that the difference in Li^+ versus Na^+ permeability is due to differences in channel affinity for the two ions, implying that the $I_{\text{Li}}/I_{\text{Na}}$ ratio strongly depends on the absolute concentration of Na^+ and Li^+ .

In the α G587A mutant, which is equally permeant to Na^+ and Li^+ , the apparent affinity for Na^+ is slightly lower and the apparent affinity for Li^+ ions is increased (Fig. 7). The K_{M} of 114 mM for Na^+ ions is close to that for Li^+ ions (90 mM) (Table IV). The α G587S mutant is characterized by a dramatic decrease in maximal conductances for Na^+ and Li^+ ions and a lower apparent K_{M} for Li^+ . The unitary Na^+ conductance of α G587S

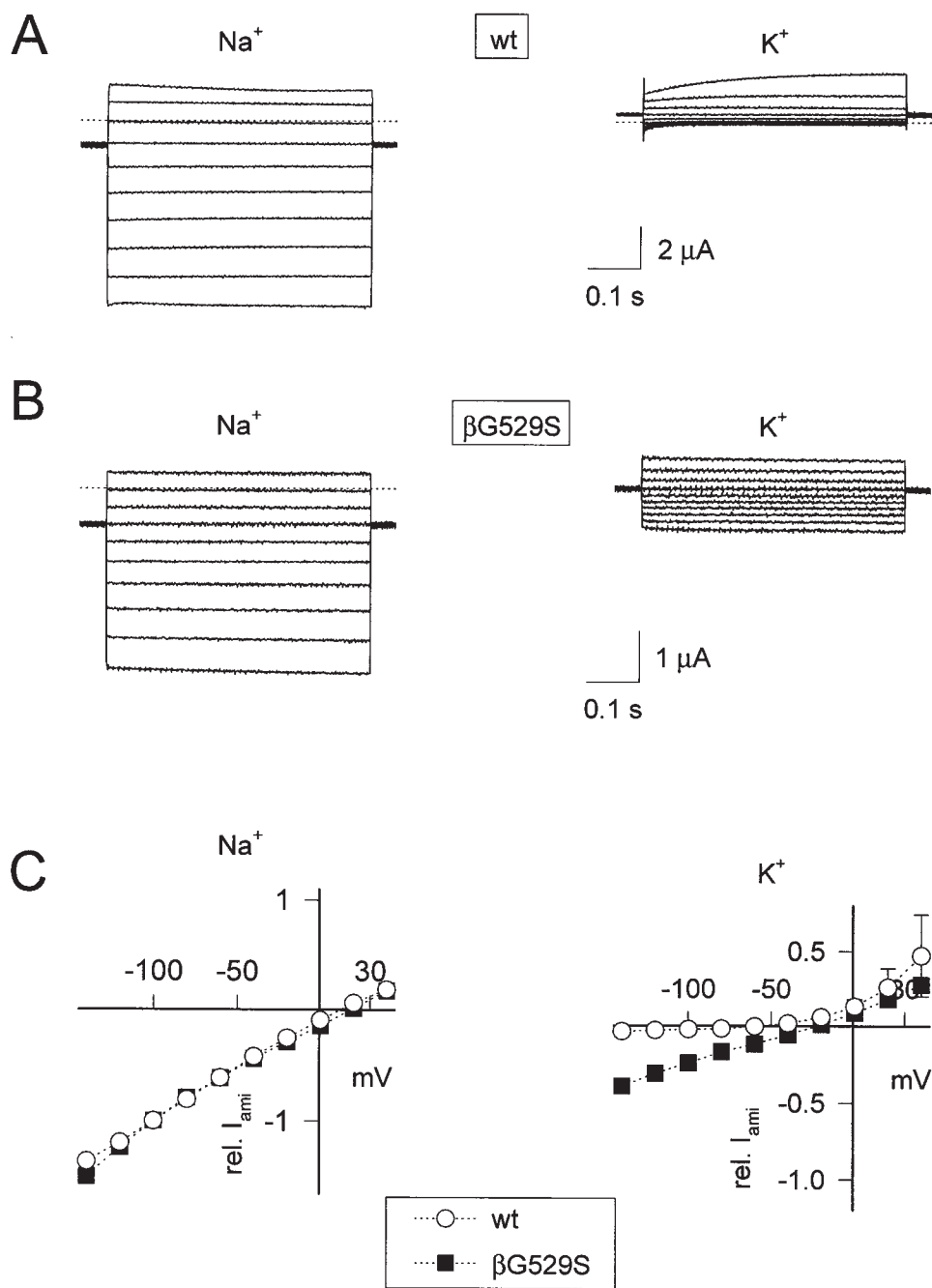


Figure 3. The β G529S mutant is partially permeable to K⁺. (A and B) Current traces of ENaC wt (A) and the β G529S mutant (B) in 40 mM Na⁺ or 120 mM K⁺ solution from two-electrode voltage-clamp recordings in *Xenopus* oocytes. Currents were measured during 500-ms voltage steps from a holding potential of -20 mV to test potentials of -140 to +40 mV in 20-mV increments. Currents measured in the presence of amiloride were subtracted from currents measured in the absence of 300 μ M amiloride, and these subtracted currents are shown. The dotted line indicates zero level of the amiloride-sensitive current. (C) The current-voltage relationship of amiloride-sensitive Na⁺ and K⁺ currents obtained as described above are shown for wt and β G529S. For each oocyte, the amiloride-sensitive current was normalized to the I_{Na} at -100 mV. I_{Na} at -100 mV was 7.8 ± 2.4 μ A for wt ($n = 4$) and 1.2 ± 0.2 μ A for β G529S ($n = 4$).

saturates at concentrations <100 mM. Due to the low g_{Na} , the K_M for Na⁺ permeation was not determined more precisely. The β G529A mutant shows a g_{Li} that saturates between 2 and 3 pS with an apparent affinity for Li⁺ ions around 40 mM, thus the apparent affinity is increased threefold compared with wt. It is remarkable that the change in apparent affinity and maximal conductance of the β G529A mutant affects only Li⁺ ions, whereas the K_M for Na⁺, and maximal g_{Na} , remained basically unchanged (Tables III and IV). Interestingly the β G529R mutation has no apparent effects on the permeation properties of Na⁺ and Li⁺ ions (Fig. 7).

The barely detectable single-channel Li⁺ currents of the γ S541A mutant (Fig. 4) made the determination of g_{Li} impossible. The γ S541A mutant showed a slight decrease in g_{Na} , with a slightly lower apparent affinity for Na⁺ ions compared with ENaC wt. Thus mutations of α G587 and β G529 change the apparent affinity for Li⁺ and/or Na⁺ ions, resulting in alterations in the single channel conductance and the microscopic conductance ratio g_{Li}/g_{Na} .

What is the affinity of the γ S541A mutant for Li⁺ ions? In a few excised outside-out macropatches, we measured macroscopic Li⁺ conductance of the γ S541A

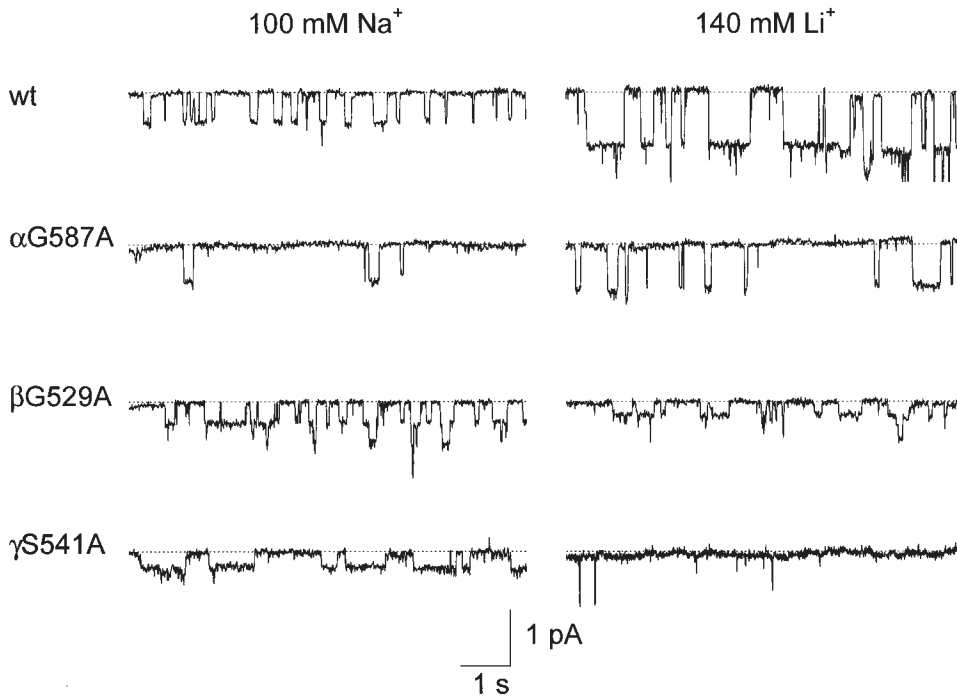


Figure 4. Single-channel Li^+ and Na^+ currents of wt ENaC and the mutants αG587A , βG529A , and γS541A . Traces are from outside-out patches from *Xenopus* oocytes at a holding potential of -100 (wt, γS541A) or -120 (αG587A , βG529A) mV at 100 mM external Na^+ or 140 mM external Li^+ . The outside-out configuration was chosen to verify amiloride sensitivity of channel activity.

mutant at five different Li^+ concentrations, and obtained an apparent K_M for Li^+ as low as 11 ± 1 mM ($n = 6$). From this high apparent channel affinity for Li^+ ions and low Li^+ permeability of the γS541A mutant, we expected that Li^+ ions should block Na^+ currents. The experiment illustrated in Fig. 8 shows that this is indeed the case. Macroscopic, amiloride-sensitive inward currents were measured in 20 mM external Na^+ and increasing Li^+ concentrations from excised outside-out macropatches from oocytes expressing the γS541A mutant. 80 mM Li^+ blocked 60% of the Na^+

current in the presence of 20 mM external Na^+ , a Na^+ concentration below the K_M for Na^+ of the γS541A mutant. The inward amiloride-sensitive current is not completely blocked by Li^+ because Li^+ still carries current in the γS541A channel. From the fit of the Li^+ inhibition curve of the I_{Na} to a simple inhibition scheme that takes into account a nonblockable fraction (see methods), we obtained an apparent Li^+ affinity for I_{Na} inhibition of 28 mM. In contrast to the situation in the γS541A mutant addition of 80 mM Li^+ to the extracellular solution increased in the ENaC wt the amiloride-

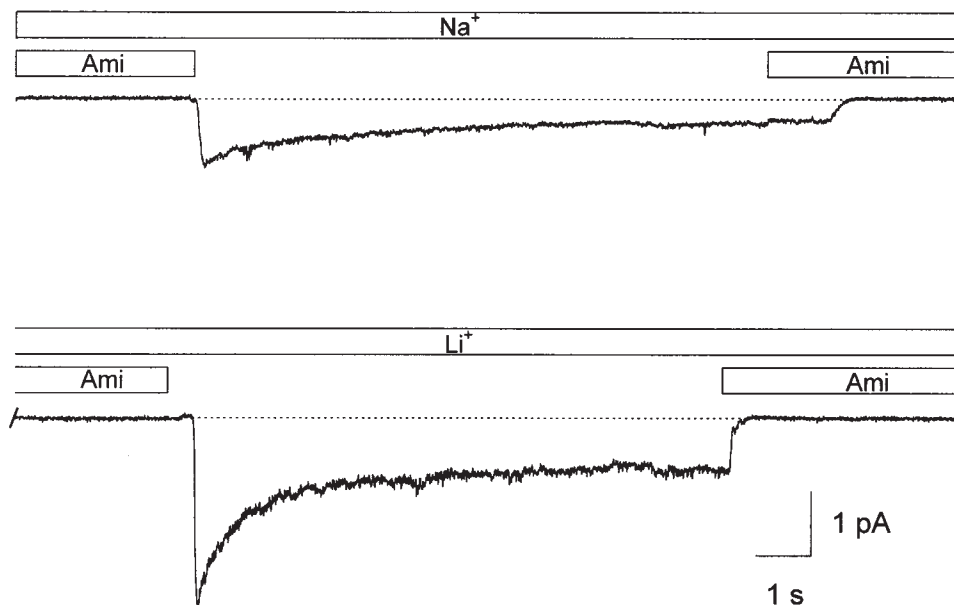


Figure 5. Amiloride-sensitive currents in macropatches from oocytes expressing the βG529S mutant. Subsequent application of extracellular Na^+ and Li^+ solution with and without 250 μM amiloride to an outside-out patch from an oocyte expressing βG529S ENaC. The holding potential was -80 mV.

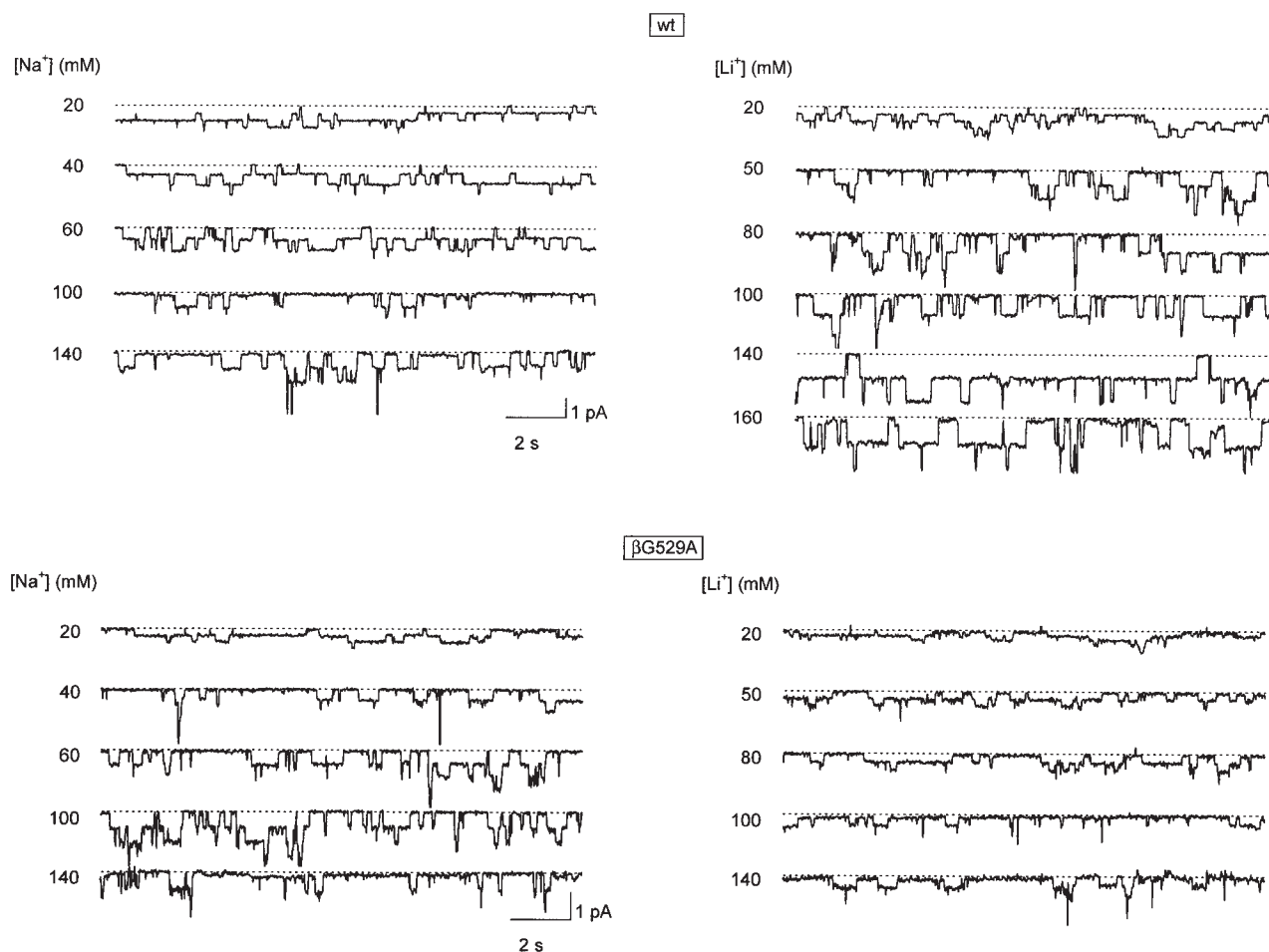


Figure 6. Ion concentration dependence of unitary currents of ENaC wt and β G529A. Single-channel recordings from outside-out patches from *Xenopus* oocytes at holding potentials of -130 (wt) or -150 (β G529A) mV in either Na^+ or Li^+ solutions. The numbers on the left side of the traces indicate the extracellular concentration of the permeant ion. Pipette solution was CsF/*N*-methyl-d-glucamine (see methods).

sensitive current by 3.1 ± 0.1 -fold ($n = 5$) at -150 mV. We conclude that the low unitary conductance of the γ S541A mutant is related to a higher apparent channel affinity for Li^+ ions.

Model of Na^+ and Li^+ Permeation in wt and Mutant ENaC

To interpret the changes in the maximal open state conductance and apparent affinity for Na^+ and Li^+ ions induced by α G587, β G529, or γ S541 mutations, we have used a simple model of ion permeation through ENaC, based on reaction rate theory of ion permeation (Alvarez et al., 1992; Hille, 1992; French et al., 1994). According to this theory, the movement of ions through the single filing region of the pore is described as a series of discrete steps between energy minima (wells), separated by energy maxima (barriers). Our model incorporates a 3B2S kinetic scheme, outlined in Fig. 9 and described in methods. Single-channel cur-

rent amplitudes, determined at various negative voltages and different concentrations of the permeant ion (either Na^+ or Li^+), were used to construct energy barrier profiles. The best fit of our I/V data and the conductance-ion concentration relationship to a 3B2S model provided energy profiles for wt and mutants shown in Fig. 9 B and listed in Table IV. The conductance-ion concentration relationship predicted by the model for the different channel types in the presence of Na^+ or Li^+ are shown as solid lines in Fig. 7. The extracellular part of the energy profile (G2, G3, U2, see Fig. 9 A) is much better defined by our data than the intracellular side (G1, U1) because we have obtained the energy barrier profiles by fitting exclusively inward currents. The best fit of our data predicts energy profiles for Na^+ and Li^+ permeation in wt ENaC that are not absolutely symmetrical, but still result in a near ohmic behavior of the I/V relationship over a voltage-range of ± 150 mV. For the wt, the higher permeability

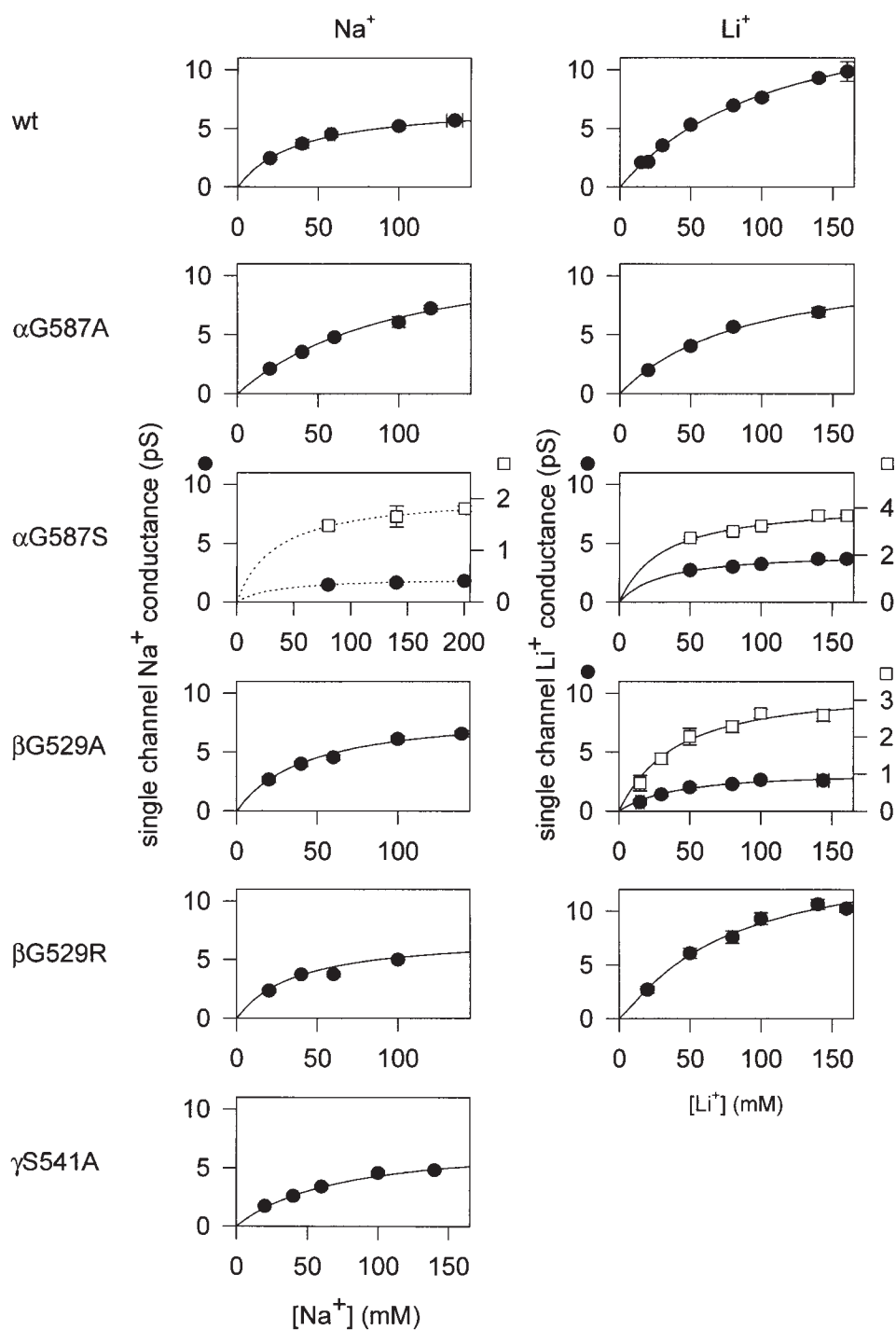


Figure 7. Saturation of single-channel conductance with increasing concentration of the permeant ion. Single-channel conductance from outside-out patches from oocytes is plotted versus the extracellular Na^+ or Li^+ concentration. Conductance was measured from a linear fit to single-channel currents at -70 , -100 , and -130 mV (wt, αG587A , βG529R) or -90 , -120 , and -150 mV (βG529A , γS541A). Each data point is from at least three different patches. In many cases, the error bars (SEM) are not visible because they are smaller than the symbol. Solid lines are the predictions by the energy barrier models (Table IV and Fig. 9). For Na^+ permeation through αG587S , the dotted lines represent a fit to the Michaelis-Menten equation. For some mutants, conductance is also shown (\square) on an expanded scale, indicated on the right hand ordinate.

of Li^+ versus Na^+ ions observed at concentrations >50 mM is mainly due to a higher energy of the outer well (U2) for Li^+ permeation, corresponding to a lower affinity for Li^+ binding.

The use of Eyring reaction rate theory has several limitations, among them the fact that it describes ion movements over well-to-well distances of fractions of Angstroms, whereas in our 3B2S model the ion translo-

cation over the three energy barriers takes place over a distance of several Angstroms. In discrete-state permeation models, the calculation of the barrier energies depends on the use of a prefactor, kT/h according to the Eyring absolute reaction rate theory (Hille, 1992; see methods). In a different approach, an approximation to a continuum model, a prefactor including the ion's diffusion coefficient and information on the ge-

TABLE IV

Energy Parameters for a 3B2S Model of Na⁺ and Li⁺ Permeation through wt and Mutant ENaC and Apparent Affinity Values to Na⁺ and Li⁺ Ions from a Fit to the Michaelis-Menten Equation

| | Na ⁺ permeation | | | | Li ⁺ permeation | | | |
|--------|----------------------------|------|------|----------------|----------------------------|-------|------|----------------|
| | U2 | G2 | G3 | K _M | U2 | G2 | G3 | K _M |
| | | | | <i>mM</i> | | | | <i>mM</i> |
| αG587A | -5.00 | 9.65 | 6.80 | 114 ± 24 | -5.50 | 9.25 | 7.05 | 90 ± 17 |
| αG587S | | | ND | | -6.80 | 8.95 | 7.05 | 35 ± 7 |
| βG529A | -7.00 | 8.05 | 6.80 | 51 ± 9 | -5.80 | 10.20 | 7.05 | 43 ± 12 |
| βG529R | -7.65 | 7.50 | 6.80 | 36 ± 13 | -9.20 | 5.10 | 7.05 | 94 ± 21 |
| γS541A | -5.35 | 9.80 | 6.80 | 71 ± 13 | -7.00 | 11.20 | 7.05 | 28 ± 2* |
| wt | -7.65 | 7.50 | 6.80 | 38 ± 6 | -6.75 | 7.50 | 7.05 | 118 ± 19 |

Single-channel I/V data at various external concentrations of Na⁺ or Li⁺ were used to obtain a 3B2S model of Na⁺ and Li⁺ permeation of wt and mutant ENaC using the AJUSTE program (Alvarez et al., 1992; French et al., 1994) as described in methods and shown in Fig. 9. Energy values (ΔG) are in RT units. The following parameters were the same for all fits: the repulsion parameter, $A = 2.6$; the electrical distance parameters, $D1 = D6 = 0.1$; $D2 = D5 = 0.15$; $D3 = D4 = 0.25$; the barrier energy, $G1 = 6.8$; and the well energy, $U1 = -4.05$. The prediction of the models for the conductance/ion concentration relationship is shown for wt and mutant ENaC as a solid line in Fig. 7. The K_M values were obtained from fits of the unitary conductance/ion concentration relationship to the Michaelis-Menten equation. *Model parameters and K_M value were obtained from the block of Na⁺ currents by external Li⁺ in macropatch experiments (Fig. 8), as described in methods.

ometry of the barrier and well has been used to calculate barrier energies (Andersen, 1989; Andersen and Koeppe, 1992). The use of this prefactor yields barrier and well energies $\sim 4.6 RT$ units more negative than the values reported in Fig. 9 B and Table IV. Because of the uncertainty about absolute energies of barriers and wells, we illustrate in Fig. 9 C the changes in barrier and well energies (G2 and U2) obtained for the αG587A, βG529A, and γS541A mutants relative to wt. These relative changes are much less model dependent. The small changes in the Na⁺ permeation through these channel mutants are simply due to a parallel positive shift in G2 and U2 (Fig. 9 C), corresponding to a slight decrease in channel affinity for Na⁺ ions but a conserved maximal g_{Na} . The gradual decrease in Li⁺ permeability and the changes in the $g_{Li}-[Li^+]$ relationship observed in αG587A, αG587S, and βG529A mutants compared with wt are essentially due to a substantial increase in the peak energy of the middle barrier (G2) relative to wt and only small changes in the energy of the outer well (U2) (Fig. 9, B and C, and Table IV). This results in a higher energy (ΔG) required for Li⁺ ions to hop over G2 from an outer binding site U2 to the inner binding site U1, and a consequently slower translocation rate of Li⁺ ions from U2 to U1.

We have used the macroscopic current data of Na⁺ current block by external Li⁺ (Fig. 8) to obtain an energy profile for Li⁺ permeation through γS541A ENaC,

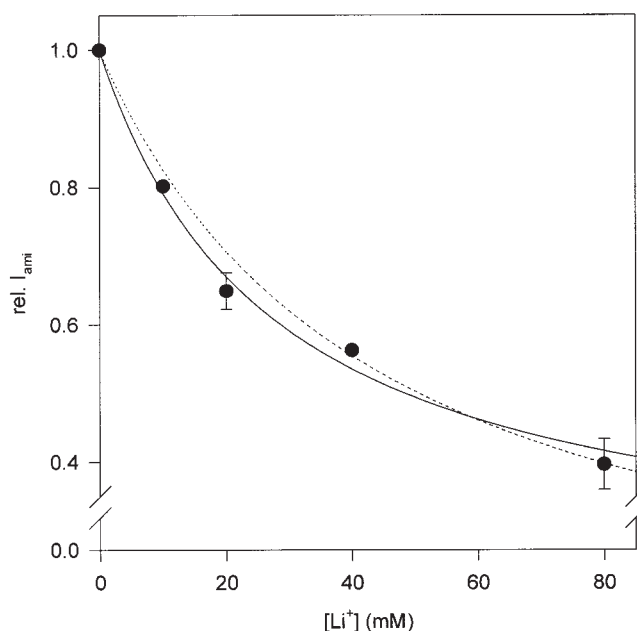


Figure 8. Block of Na⁺ current through γS541A ENaC by increasing concentrations of external Li⁺. Data are from outside-out macropatch recordings at a holding potential of -150 mV from *Xenopus* oocytes expressing γS541A. The bath solution contained 20 mM Na⁺ and increasing concentrations of Li⁺. The amiloride-sensitive currents were normalized to the condition without Li⁺ ($n = 3$ for each data point), shown as mean \pm SEM. The fit to a simple inhibition scheme (see methods) taking into account a non-blockable fraction (= Li⁺ current) yielded an apparent K_i of 28 mM and is shown as a solid line. The prediction by the 3B2S model (see Table IV and methods) is shown as a dotted line.

as described in methods. The prediction of the Li⁺ block by the model is shown as a dotted line in Fig. 8, and the energy parameters for the fit are listed in Table IV and shown in Fig. 9 B. As for the αG587A and βG529A mutants, the corresponding energy profile predicted for Li⁺ permeation through γS541A shows a higher peak energy of the middle energy barrier that increases the energy required for translocation of Li⁺ ions from U2 to U1 (Fig. 9, B and C). Thus, when Li⁺ occupies the pore of the γS541A in the single filing region, it slows the movement of Na⁺ ions.

Is the Pre-M2 Segment the Specific Target Region for Amiloride Block and Na⁺/Li⁺ Selectivity?

The question remains as to whether amiloride binds to a unique site in the external pore, and whether the ion selectivity filter is confined to the region we identified in the pre-M2 segment. Recently, Ismailov et al. (1997) identified a WYRFHY sequence rich in aromatic residues in the large extracellular loop of αENaC as a putative amiloride-binding domain. Later, it was reported that conserved Lys residues at positions 550 and 561 in αENaC are critical for channel sensitivity to amiloride

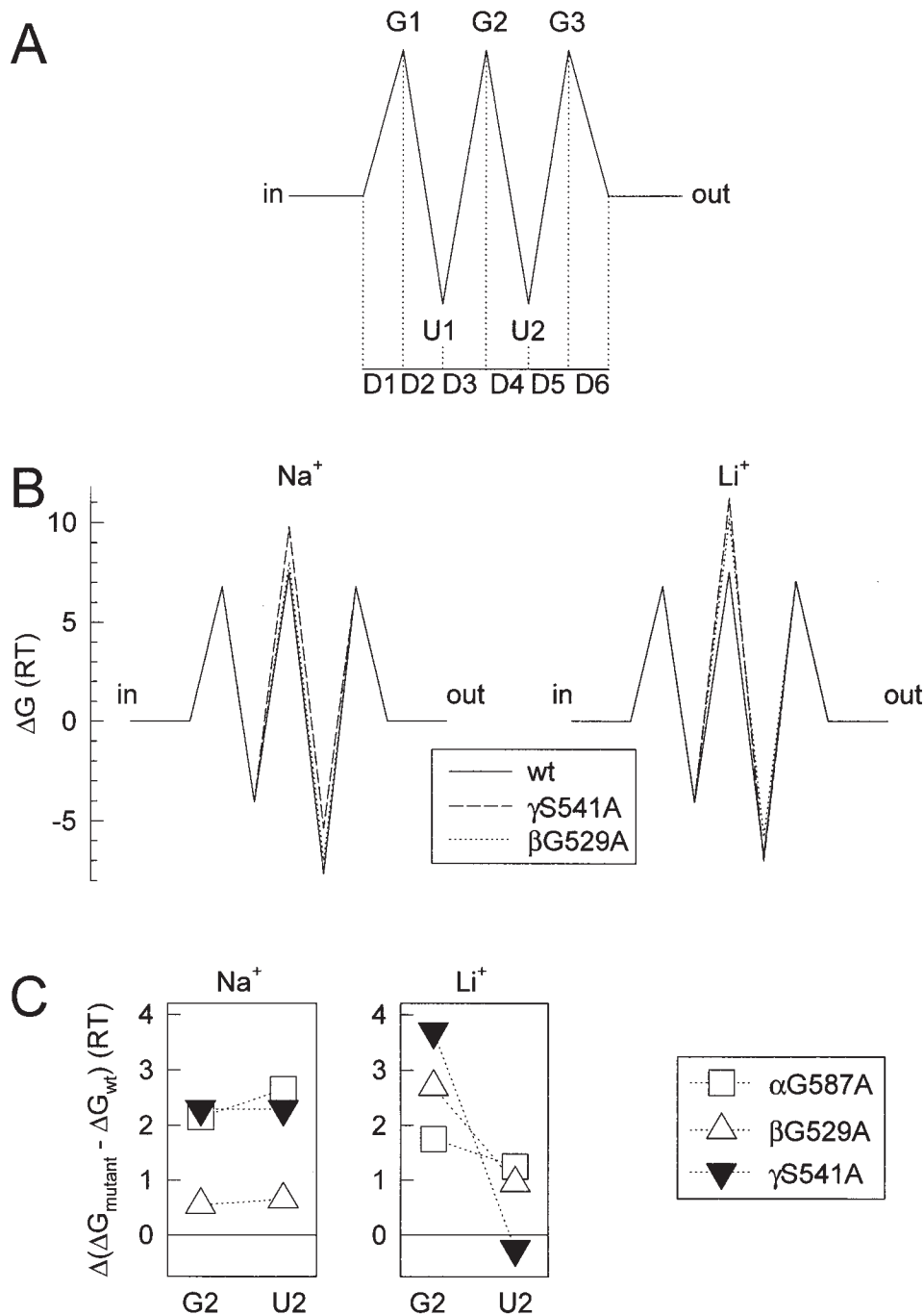


Figure 9. Energy barrier models of Na⁺ and Li⁺ permeation through open wt or mutant ENaC. (A) Parameters of the 3B2S model are represented and include: peak energies (G1-G3), well energies (U1, U2), and electrical distances (D1-D6). (B) Energy diagrams are drawn according to best-fit parameter values for the 3B2S model listed in Table IV. Profiles for wt (solid line), βG529A (dotted line), and γS541A (dashed line) are shown. (C) The ΔG changes relative to wt ($\Delta[\Delta G_{\text{mutant}} - \Delta G_{\text{wt}}]$) of G2 and U2, the free parameters in the model fitting, are shown for αG587A, βG529A, and γS541A.

and for ion selectivity (Fuller et al., 1997). Since these studies were done on channels presumably made of αENaC subunits reconstituted in lipid bilayers, we tested the relevance of these mutations for the pharmacological and functional properties of ENaC composed of the three types of subunits, α, β, and γ.

Following expression of an α mutant with deletion of the WYRFHY sequence together with β and γ subunits, no I_{Na} could be measured and no ENaC cell surface expression could be detected using anti-FLAG antibodies

directed against β and γ subunits. The point mutation within this sequence, αH282D, reported to be responsible for ENaC insensitivity to amiloride did not result in changes in amiloride sensitivity or macroscopic ionic selectivity of channels made of αH282Dβγ (Tables II and III). The αK550E and the αK561E mutants, when coexpressed with β and γ subunits, exhibited the same sensitivity to block by amiloride as ENaC wt and showed normal macroscopic Na⁺/Li⁺ selectivity and unitary currents (Tables I-III). From these results, we conclude

that the putative amiloride-binding sequence described by Ismailov et al. (1997) and the Lys residues in the large extracellular loop (Fuller et al., 1997) are not relevant for the amiloride sensitivity and ionic selectivity of the native ENaC made of α , β , and γ subunits.

discussion

Our mutagenesis experiments have identified amino acid residues at homologous positions in α , β , and γ ENaC subunits, located two residues upstream of the predicted NH₂ terminus of the second transmembrane α helix, that play an important role in ion conduction. Mutations of these residues α G587, β G529, and γ S541 resulted in the following changes in ion permeation and channel ionic selectivity. First, the mutations α G587D, γ S541N, γ S541F, and γ S541R resulted in channels, which were expressed at the cell surface at normal densities, but did not conduct ionic current or showed only a minuscule ionic current (γ S541R). Second, α G587A, β G529A, β G529C, and γ S541A mutations decreased Li⁺ permeability with relatively small changes in Na⁺ permeability. Third, introduction of a Ser residue in the α (α G587S) and β subunits (β G529S) resulted in a decrease in both Na⁺ and Li⁺ unitary currents with no apparent changes in the Li⁺/Na⁺ permeability ratio. Fourth, the β G529S (and similarly β G529C and β G529D) mutant was permeant to K⁺ ions and to a lesser extent to Rb⁺ ions. Finally, the mutants α G587S, β G529A, β G529C, and β G529S with major changes in ion permeation or selectivity also showed resistance to amiloride block. These observations indicate that α G587, β G529, and γ S541 interact closely with the permeant Na⁺ and Li⁺ ions, and participate at least in part in ion discrimination at the selectivity filter. The selectivity filter appears in close vicinity of the amiloride binding site.

The amiloride-sensitive ENaC, target of aldosterone action in the distal nephron and colon, is made of homologous $\alpha\beta\gamma$ subunits. This channel is highly selective for Na⁺ over K⁺ ions and has the unique characteristic among the other members of the ENaC/DEG gene family of being more permeant to Li⁺ than to Na⁺ ions. The higher permeability of ENaC for Li⁺ compared with Na⁺ ions was evident from early macroscopic current measurements in flat epithelia like frog skin or toad urinary bladder. In these preparations, it was generally not possible to detect currents through ENaC carried by K⁺ ions. The only ion other than Na⁺ and Li⁺ allowed to pass through the channel was H⁺. The selectivity profile H⁺ > Li⁺ > Na⁺ of ENaC suggested that the pore discriminates among cations mainly on the basis of the size of the dehydrated ion allowing small cations to pass through the channel. Larger cations such as K⁺, Rb⁺, or Cs⁺ go only part-way along the

ion conduction pathway, and block the channel pore at high concentrations, but are not able to pass the most constricted region of the pore, the selectivity filter (Palmer, 1990; Garty and Palmer, 1997).

In support of this hypothesis for ion selectivity in ENaC is our recent finding that mutation of the highly conserved α S589 residue alters the molecular sieving properties of ENaC (Kellenberger et al., 1999). Specific α S589 mutants exhibit different I_K/I_{Na} ratios. In particular, the α S589D mutant with the highest K⁺/Na⁺ permeability ratio showed a permeability profile for alkali metal cations following the order K⁺ > Rb⁺ > Cs⁺, indicating that α S589 mutations result in an increase in the molecular cutoff of ENaC. It was concluded that α S589 is part of the selectivity filter, which acts as a molecular sieve to discriminate between small Na⁺ or Li⁺ ions and larger K⁺ ions.

In the present study, the mutants that show a significant K⁺ permeability are β G529S, β G529C, and β G529D; the permeability relative to Na⁺ of these mutants was higher for K⁺ ions than for Rb⁺, and no current carried by Cs⁺ could be detected. The increase in the channel molecular cutoff by the β G529 mutations is consistent with the notion that, like the α S589 mutation, they enlarge the pore diameter at the selectivity filter and alter the molecular sieving properties of the channel (Kellenberger et al., 1999). Thus the changes in the pore geometry at the selectivity filter that allow K⁺ or Rb⁺ ions to pass through the pore can be achieved by specific mutations of α S589 or β G529 residues. It suggests that these two residues are important for the steric selectivity of the channel by maintaining the proper pore geometry to tightly accommodate the permeating ion and exclude larger ions.

Beside the changes in ion selectivity of the β G529S, β G529C, and β G529D mutants, mutations of the α G587, β G529, and γ S541 residues resulted in important changes in the permeability properties of the channel for Na⁺ and Li⁺ ions. These effects involve both the changes in the maximal open state conductance (Fig. 7) and/or in the apparent channel affinity for Na⁺ and Li⁺ ions as determined by K_M values for channel conductance. Recordings of individual channels in the native tissue have shown that the open state conductance of ENaC saturates with increasing concentrations of Na⁺ and Li⁺ ions, indicating that Na⁺ and Li⁺ ions bind to specific sites in the ion permeation pathway. This saturation process arises when the binding-unbinding steps of the ion conduction at specific binding sites along the pore become rate limiting. At high ion concentrations, the channel pore is occupied most of the time and the rate of ion translocation is determined by the maximal rate at which the permeant ions dissociate from their binding site and the ion flux approaches saturation. For ENaC wt, the dependence

of open state conductance on the concentration of the conducting ion gives an apparent affinity (K_M) of 38 mM for Na^+ and 118 mM for Li^+ . This difference in channel affinity for Na^+ and Li^+ ions can account for the higher Li^+ over Na^+ permeability usually observed at an ion concentration around 100 mM since the flux of Na^+ ions already reaches saturation at these concentrations (see Fig. 7). Specific binding sites for Na^+ have been postulated on the basis of competitive interactions between Na^+ and amiloride or K^+ ions that inhibit Na^+ current through the channel in a voltage-dependent manner. In addition, the lack of voltage dependence of channel occupancy by Na^+ ions was consistent with the presence of multiple ion binding sites along the channel pore. Reasonable models for Na^+ permeation have been proposed that are consistent with these experimental observations. These models involve at least two common binding sites for Na^+ , Li^+ , K^+ , and amiloride in the outer mouth of the channel (Palmer, 1990).

How can the decrease in Li^+ permeability relative to Na^+ of the αG587A , βG529A , or γS541A mutants be explained in molecular terms? High affinity binding of ions in the channel pore tends to slow ion permeation provided that the channel is occupied by a single ion at a time. A low Li^+ permeability was observed in αG587A , βG529A , or γS541A mutants characterized by a lower maximal g_{Li} and an apparent higher affinity for Li^+ compared with wt. Alternatively, the mutations might result in steric changes within the narrow region of the pore, making it more difficult for Li^+ ions to pass through. For the interpretation of the changes in ion permeation in ENaC mutants, we need to consider ion conduction through ENaC consisting basically of three fundamental processes: (a) diffusion of an ion up to the outer entrance of the channel pore, (b) dehydration and solvation of the ion by polar chemical groups lining the pore, and (c) translocation through the selectivity filter. Models of ion permeation in terms of energy profile and Eyring rate theory can formulate these processes (Hille, 1992). We have empirically chosen an energy profile for Na^+ and Li^+ translocation through ENaC that consists of two energy wells representing two binding sites and three energy barriers for ion translocation. It has previously been shown that this type of model (3B2S) for ion conduction can account for the electrical properties of ENaC (Palmer and Andersen, 1989). In energy barrier models, the K_d of the permeant ion is defined by the value of the deepest energy well; thus, the deeper the well, the lower the concentration needed to reach saturation of the ion flux. By contrast, the higher the energy barriers, the lower the maximal conductance of the channel. While such models cannot provide an accurate representation of the structure of the ion conduction pathway, they can help us to

determine whether alterations in ion conduction of αG587A , βG529A , or γS541A mutants can be related to particular permeation mechanisms. In the ENaC wt, the energy barrier profile obtained for Li^+ permeation compared with Na^+ is characterized by a higher outer energy well consistent with a lower affinity for Li^+ at an external binding site (Fig. 9 and Table IV), accounting for the differences in Li^+ versus Na^+ permeability. In our models for Li^+ permeation through the αG587A , βG529A , or γS541A mutants, the predominant changes in Li^+ versus Na^+ conductance are due to an increase in the middle energy barrier, with little changes in the outer energy well. It suggests that translocation of Li^+ ions in the single filing region at the central energy barrier requires more energy in mutants compared with wt. Thus, the αG587 , βG529 , or γS541 residues can be assigned to a region of the pore that represents a significant barrier for ion translocation. It is possible that βG529 and γS541 have preferential interactions with Li^+ ions since mutations of these residues did not affect Na^+ permeation much.

We observed that the βG529S , βG529C , and βG529D mutations change the channel molecular cutoff allowing K^+ and Rb^+ ions to pass through the channel. Thus, βG529 plays a role in defining the molecular cutoff of the channel and is at the same time important for the Li^+/Na^+ selectivity. The dual role of βG529 underlines that the discrimination between Li^+ and Na^+ , and between Na^+ and larger ions, occurs at overlying sites in the selectivity filter. Our data suggest that αG587A , βG529A , and γS541A mutations result in steric changes at the selectivity filter that impair translocation of Li^+ ions through the narrowest part of the channel pore. In moving from the outer binding site U2 into the narrowest region of the pore, the permeant ion likely has to lose a few more molecules of its hydration shell. This loss of the hydration shell raises the energy of the permeant ion. Our data are consistent with the hypothesis that the energy cost for Li^+ dehydration at the U2 \rightarrow G2 translocation is raised in the αG587A , βG529A , and γS541A mutants because it cannot be sufficiently compensated by the interactions between the permeant ion and the polar groups lining the pore. Mutations such as αG587S and βG529S decrease unitary conductance for both Na^+ and Li^+ ions, although the low unitary currents made it difficult for αG587S and impossible for βG529S to fit the I/V data to our 3B2S model. The energy profile of αG587S for Li^+ conduction predicts an increased peak energy of the middle barrier, consistent with what we observed for the other mutants discussed above. The conductance data of βG529S are also compatible with a mutation resulting in a considerable increase in the peak energy of the middle barrier for Na^+ and Li^+ permeation, but a decrease in the energy barrier for K^+ conduction. The binding site U2 cannot be

assigned yet to a molecular structure, but is likely to be in the close vicinity of the selectivity filter.

It is somewhat surprising that the effects of substitutions of α G587, β G529, and γ S541 did not correlate in a predictable way with general physical-chemical properties of the substituting amino acid residues. The fact that ion permeation is not altered by the β G529R mutation indicates that charges do not play a crucial role in ion coordination at the selectivity filter, and basically excludes the possibility that the β G529 side chain faces the lumen of the channel pore. As already suggested for α S589 mutations (Kellenberger et al., 1999), the amino acid side chain of β G529 (and probably of its analogues) are likely to point away from the channel pore, in a similar way as has been shown for the selectivity filter of the KcsA channel (Doyle et al., 1998). If this is the case, the side chains of these amino acid residues are likely to interact with other amino acid residues, to keep the backbone of α G587, β G529, and γ S541 in place and maintaining the proper conformation of the pore at the selectivity filter. In ENaC wt, Gly, and Ser, amino acid residues with short side chains make these interactions, and the positive charge in the β G529R mutant (four carbon atoms between the α -carbon atom and NH_3 group) might be too far away to disrupt this interaction. In mutant channels that are permeable to K^+ (α S589 and some β G529 mutants), the mutated side chain might push parts of the pre-M2/M2 domains of the subunits away from each other or tilt them, resulting in a widening of the pore.

In summary, our mutagenesis experiments indicate that α G587, β G529, γ S541, and α S589 residues are part of the narrow region of the pore that constitutes the selectivity filter of ENaC (Fig. 1 C). It seems that the important steps of ion conduction that involve ion dehydration, solvation, and translocation occur in a very restricted region of the ion permeation pathway that encompasses the α G587 and analogues and α S589 residues. For comparison, the crystal structure of the KcsA channel reveals that the narrow selectivity filter lined by the backbone of VGYG residues is only 12-Å long,

whereas the overall length of the pore is 45 Å (Doyle et al., 1998).

Finally, the mutations α G587S, β G529A, and β G529S that change ion selectivity and ion permeation properties also decrease channel affinity for amiloride, whereas the β G529 mutation without consequences on ion permeation properties did not change channel blocking by amiloride. It is unlikely that α G587 and β G529 are involved in specific binding interactions with amiloride since nonconserved substitutions have no effect on channel affinity for amiloride. The α G587A, β G529A, or γ S541A mutations may indirectly impair the binding interaction of amiloride with the channel pore by steric changes that result in alterations in the pore geometry. According to its size, amiloride is not supposed to penetrate deep into the narrowest part of the selectivity filter. We propose that α G587 and β G529 are located at the external entrance of the narrow selectivity filter where steric alterations of the pore have consequences on amiloride binding in the channel outer vestibule.

Fig. 1 C, showing the ion pore of ENaC, illustrates some relevant experimental observations regarding the structures involved in ion conduction. The Gly 525 and 537 residues of β and γ subunits and to a lesser extent the corresponding α S583 residue form the amiloride binding site in the pore (Schild et al., 1997). Mutation of the two α S583 residues in the ENaC tetramer to Cys creates a high-affinity binding site for Zn^{2+} (Firsov et al., 1998). Because the α subunits are most likely on opposite sides of the channel pore (Firsov et al., 1998), and the optimal distance of two sulfhydryl groups for coordinated ligation of Zn^{2+} is ~ 5 Å (Krovetz et al., 1997), we estimate the pore diameter at this site to be around 5 Å. The pore then narrows down to its narrowest part that constitutes the selectivity filter. This narrow region is relatively short and may be lined by only three amino acid residues involving the residues Ser or Gly in the $\alpha\beta\gamma$ subunits. We suggest that, in analogy to the KcsA channel, the cytoplasmic part of the pore is lined by residues from the second transmembrane α helix.

We thank B.C. Rossier, J.-D. Horisberger, and P. Greasley for helpful comments on the manuscript

This work was supported by grant 31-49654.96 from the Swiss National Foundation for Scientific Research (L. Schild).

Submitted: 5 March 1999 Revised: 23 April 1999 Accepted: 30 April 1999

references

- Alvarez, O., A. Villarroel, and G. Eisenman. 1992. Calculation of ion currents from energy profiles and energy profiles from ion currents in multibarrier, multisite, multioccupancy channel models. *Methods Enzymol.* 207:816-854.
- Andersen, O.S. 1989. Kinetics of ion movement mediated by carriers and channels. *Methods Enzymol.* 171:62-112.
- Andersen, O.S., and R.E. Koeppe II. 1992. Molecular determinants of channel function. *Physiol. Rev.* 72:S89-S158.
- Canessa, C.M., A.-M. Merillat, and B.C. Rossier. 1994a. Membrane topology of the epithelial sodium channel in intact cells. *Am. J. Physiol.* 267:C1682-C1690.
- Canessa, C.M., L. Schild, G. Buell, B. Thorens, I. Gautschi, J.-D.

- Horisberger, and B.C. Rossier. 1994b. Amiloride-sensitive epithelial Na⁺ channel is made of three homologous subunits. *Nature*. 367:463–467.
- Doyle, D.A., J.M. Cabral, R.A. Pfuetzner, A.L. Kuo, J.M. Gulbis, S.L. Cohen, B.T. Chait, and R. MacKinnon. 1998. The structure of the potassium channel—molecular basis of K⁺ conduction and selectivity. *Science*. 280:69–77.
- Firsov, D., I. Gautschi, A.M. Merillat, B.C. Rossier, and L. Schild. 1998. The heterotetrameric architecture of the epithelial sodium channel (ENaC). *EMBO (Eur. Mol. Biol. Organ.) J.* 17:344–352.
- Firsov, D., L. Schild, I. Gautschi, A.-M. Mérellat, E. Schneeberger, and B.C. Rossier. 1996. Cell surface expression of the epithelial Na channel and a mutant causing Liddle syndrome: a quantitative approach. *Proc. Natl. Acad. Sci. USA*. 93:15370–15375.
- French, R.J., J.F. Worley III, W.F. Wonderlin, A. Shavantha Kularatna, and B.K. Krueger. 1994. Ion permeation, divalent ion block, and chemical modification of single sodium channels. Description by single- and double-occupancy rate-theory models. *J. Gen. Physiol.* 103:447–470.
- Fuller, C.M., B.K. Berdiev, V.G. Shlyonsky, I.I. Ismailov, and D.J. Benos. 1997. Point mutations in α -bENaC regulate channel gating, ion selectivity, and sensitivity to amiloride. *Biophys. J.* 72:1622–1632.
- Garty, H., and L.G. Palmer. 1997. Epithelial sodium channels—function, structure, and regulation. *Physiol. Rev.* 77:359–396.
- Hille, B. 1992. *Ionic Channels of Excitable Membranes*. 2nd ed. Sinauer Associates, Inc., Sunderland, MA.
- Ismailov, I.I., T. Kieberemmons, C.M. Lin, B.K. Berdiev, V.G. Shlyonsky, H.K. Patton, C.M. Fuller, R. Worrell, J.B. Zuckerman, W. Sun, et al. 1997. Identification of an amiloride binding domain within the alpha-subunit of the epithelial Na⁺ channel. *J. Biol. Chem.* 272:21075–21083.
- Kellenberger, S., I. Gautschi, and L. Schild. 1999. A single point mutation in the pore region of the epithelial Na⁺ channel changes ion selectivity by modifying molecular sieving. *Proc. Natl. Acad. Sci. USA*. 96:4170–4175.
- Krovetz, H.S., H.M.A. VanDongen, and A.M.J. VanDongen. 1997. Atomic distance estimates from disulfides and high-affinity metal-binding sites in a K⁺ channel pore. *Biophys. J.* 72:117–126.
- Lingueglia, E., G. Champigny, M. Lazdunski, and P. Barbry. 1995. Cloning of the amiloride-sensitive FMRamide peptide-gated sodium channel. *Nature*. 378:730–733.
- Palmer, L.G. 1982. Na⁺ transport and flux ratio through apical Na⁺ channels in toad bladder. *Nature*. 297:688–690.
- Palmer, L.G. 1990. Epithelial Na channels: the nature of the conducting pore. *Renal Physiol. Biochem.* 13:51–58.
- Palmer, L.G., and O.S. Andersen. 1989. Interactions of amiloride and small monovalent cations with the epithelial sodium channel. Inferences about the nature of the channel pore. *Biophys. J.* 55:779–787.
- Renard, S., E. Lingueglia, N. Voilley, M. Lazdunski, and P. Barbry. 1994. Biochemical analysis of the membrane topology of the amiloride-sensitive Na⁺ channel. *J. Biol. Chem.* 269:12981–12986.
- Schild, L., E. Schneeberger, I. Gautschi, and D. Firsov. 1997. Identification of amino acid residues in the α , β , γ subunits of the epithelial sodium channel (ENaC) involved in amiloride block and ion permeation. *J. Gen. Physiol.* 109:15–26.
- Tavernarakis, N., and M. Driscoll. 1997. Molecular modeling of mechanotransduction in the nematode *Caenorhabditis elegans*. *Annu. Rev. Physiol.* 59:659–689.
- Waldmann, R., G. Champigny, F. Bassilana, N. Voilley, and M. Lazdunski. 1995a. Molecular cloning and functional expression of a novel amiloride-sensitive Na⁺ channel. *J. Biol. Chem.* 270:27411–27414.
- Waldmann, R., G. Champigny, and M. Lazdunski. 1995b. Functional degenerin-containing chimeras identify residues essential for amiloride-sensitive Na⁺ channel function. *J. Biol. Chem.* 270:11735–11737.
- Waldmann, R., and M. Lazdunski. 1998. H⁺-gated cation channels—neuronal acid sensors in the ENaC/DEG family of ion channels. *Curr. Opin. Neurobiol.* 8:418–424.